地震研究所彙報
Bull. Earthq. Res. Inst.
Univ. Tokyo
Vol. 71 (1996) pp. 1-45

Computer Simulations of Dynamic Fracture and Rupture Propagation

Mahesh Raj Rimal Obayashi Corporation (Formerly at the ERI, The Univ. of Tokyo)

(Received January 22, 1996)

Abstract

Numerical simulations of fractures of the Earth's crust are made using the Extended Distinct Element Method (EDEM), which has been found to be suitable for simulating the behavior of a medium from a continuous state to a discrete state following the total fracture process. Two sets of numerical experiments are conducted: 1) the boundaries of a model are sheared to cause a fracture; 2) the state just prior to the rupture of the Earth's crust is simulated first and then parameterization is done to incite a rupture. From the first set of experiments, progressive development of cracks inside the medium and dilatation as a result of pervasive cracks are simulated. The shear forces show a stick-slip type of behavior. From the second set of tests, it has been possible to simulate rupture propagation from the region where it is incited. The effects of having strength barriers ahead of the advancing rupture edge are studied. Several types of barrier, depending upon their strength distributions, are considered. The rupture speed is seen to decrease with the increase of barrier strength and in the case of a barrier having random strength distribution, rupturing is found to stop after having propagated in a zigzag manner for some distance. Finally, stress drop due to the rupture and the mechanism for starting the rupture are studied with two experiments using EDEM. In spite of the qualitative nature of the results, they are first obtained by such an approach and emphasis is more on the method and need for its development for quantitative studies in the future.

1. Introduction

The physics of earthquake focus, in essence, is the physics of collapsing rock masses in the environment of the Earth's interior. Studying the physics of earthquake focus is rather complicated. The processes of rapid fracture spread and its arrest are of interest to a seismologist. As distinct from the engineering discipline, seismological studies demand a study of growths of a large number of fractures in a heterogeneous medium. Strength heterogeneity of the medium is primarily responsible for the arrest of fractures. The mechanism whereby fracturing stops also constitutes an active area of research. Arresting a rupture with a strength barrier, beyond which is an area under high stresses, causes the process to linger with strong aftershocks. Extension of the fault to the area under low average stresses is responsible for fault cessation. These phenomena are studied by many researchers using different approaches.

The development of various useful experimental techniques and advances in computer systems have greatly helped us to increase our knowledge in the field of fault mechanics. Three approaches, namely, theoretical, experimental, and numerical approaches, used to model an earthquake source and the relevant literatures are reviewed in the following section. Problems related to fracturing of the Earth's crust are complicated and there is no unified approach to solving them. After this brief review there is a description of the computational method used in this study and the simulation of dynamic fracture of the crust and rupture propagation considering barrier regions ahead of the advancing rupture edge.

1.1 Laboratory Approach

In this approach, the results of experiments on rock specimens, foam rubber models and/or wooden boards are obtained and inferences are made about earthquakes. Kishinoue (1937) used thin wooden boards with regular grains having heterogeneous and somewhat brittle characteristics to model earthquake and showed that the fracture mode resembled the mode of occurrence of an earthquake swarm. Savage et al. (1963) observed the radiation pattern of elastic waves from a tensile fracture in a 2-D glass model in which the fracture was induced by a local concentration of thermal stresses. He was able to obtain only qualitative agreement of his results with the previous theoretical work and concluded that the disagreement in terms of quantitative results was due to nonlinear processes inherent in the fracture. Brace and Byerlee (1966) showed that previously faulted surfaces of rock may undergo a series of intermittent small slips under continuing pressure, which they called stick-slip, and suggested this mechanism might apply to earthquakes. Mogi (1967) conducted experiments on rocks and proposed his fracture theory of earthquakes to explain various types of sequences of earthquakes from the results of his experiments. He concluded in his paper that the acoustic emission (AE) characteristics in the case of a heterogeneous model were similar to the occurrence of swarms of earthquakes. Scholz (1968) showed that during deformation of rock in laboratory experiment, micro-fractures radiated elastic waves in a manner similar to earthquakes and that their frequency-magnitude relation was found to obey the Gutenberg and Richter relation. He concluded that micro-fractures in rock specimens in the laboratory could be a basis for studying various earthquake phenomena. Brune (1973) used foam rubber models for earthquake modeling. He concluded that stick-slip along precut fault surfaces in stressed foam rubber has many of the characteristics of earthquake slip along faults in the Earth and that foam rubber models might be used to study strong motions around various types of faults. Brady (1974) and Stuart (1974) used dry models of dilatation cracks to explain the basic features of seismic precursors.

1.2 Theoretical and Numerical Approaches

In the theoretical approach, the rupture process is modeled as two- and three-dimensional propagating dynamic shear cracks, incorporating initial stress field and static and sliding frictional strengths of the fault surface. There have been a lot of studies simulating the rupture of an earthquake and when compared to contemporary models the earliest theoretical model proposed for fault mechanics is extremely simple. It simulates a strike-slip vertical fault with an infinitely long strip intersecting the surface of an elastic semi-infinite medium, which is under uniform strain (Kasahara, 1957; Knopoff, 1958). The scope of fault studies was widened remarkably by the introduction of dislocation theory (Stekette, 1958 a,b; Maruyama, 1973) into this research field by considering an earthquake fault as a huge dislocation in the Earth. Crack theory or fracture mechanics was applied after Kostrov (1966) discussed the dynamics of crack extension for a semi-infinite longitudinal shear crack. Takeuchi and Kikuchi (1973) extended Kostrov's method and discussed the physics of the earthquake process. These analytical methods have provided an insight into the general features of dynamical crack propagation, but are reported to be incapable of dealing with more realistic distributions of shear stress and strength.

Recent progress in computer technology has led to the development of simulation

techniques providing us with powerful ways of simulating many complicated phenomena and the scope of field of seismology has been greatly widened. A computer model is constructed and the responses of the model are compared to direct observations. Burridge and Knopoff (1967) constructed both laboratory and numerical models to explore the role of friction along a fault as a factor in the earthquake mechanism. They proposed a one-dimensional model which simulates a fault with a group of discrete mechanical elements associated with mass, elasticity, friction and viscosity to explain repeated fault slips under stress. Andrews (1976 a,b) calculated the propagation of two-dimensional in-plane shear cracks and obtained terminal rupture velocities. Madariaga (1976) solved the problem of a circular crack that expanded with a constant velocity and stopped. Yamashita (1976), Miyatake (1977) and Mikumo and Miyatake (1978) studied spontaneous rupture propagation on a three-dimensional fault. Das and Aki (1977) used a barrier model and considering the problem of unilateral propagation of rupture, showed that shear cracks with finite cohesive forces can propagate by skipping past barriers. Miyatake (1980 a,b) treated rupture propagation using a three-dimensional finite difference method. Toki and Miura (1985) simulated the fault rupture mechanism with a two-dimensional finite element method, using joint elements. Zhiren and Dangmin (1988) studied slip-weakening instability on a finite and vertical strike-slip fault with asperity as a plane-stress problem using the finite element method. Ohnaka and Yamashita (1989) investigated local breakdown processes near the propagating tip of the slipping zone under the mode II crack growth condition to understand the constitutive behavior near the rupture front during an earthquake shear failure along a pre-existing fault. Brown et al. (1991) constructed a cellular automaton model of earthquakes which describes the time evolution of a two-dimensional system of coupled masses and springs sliding on a frictional surface. The model was shown to exhibit power-law frequency relations like those in earthquakes. Mora and Donze (1992) presented a lattice model of the nonlinear dynamics of earthquakes.

The finite element method is used by some researchers (see, for example, Toki et al., 1985) to study rupture propagation. The difficulty in using the finite element method to model earthquake source process lies in the fact that in spite of using joint elements, attachment of a node to another previously unconnected node—as a result of a large movement—cannot be easily implemented. The Rigid Body Spring Model (RBSM) proposed by Kawai T. bears similarity with the finite element method in that the contacting elements are specified, separation is not allowed and hence, new contact between elements which were not in contact before cannot be simulated. Regarding the finite difference method, it has the weak point in that the grid points cannot displace so that only temporal variations can be studied. However, the Extended Distinct Element Method (EDEM), being able to simulate the behavior of a medium from a continuous stage to a discontinuous stage following the total fracture process, can simulate progressive development of cracks inside a medium in a natural way. It also allows the movement of elements both in space and time, so that adjacent sides of the fault can fling past each other when the rupture edge passes through the interface. Therefore, a study of fracture of the Earth's crust can be thought to be a potential field in terms of its applications.

2. Computational Method

The Distinct Element Method (DEM), which is applicable only to discrete granular assemblies, was originally put forward by Cundall (1971) and has since then been modified and applied to many fields. This method is based on an explicit numerical scheme in which the motion of every particle in a granular assembly is calculated based on the laws of motion. At each time step, forces acting on a particle from the surrounding particles are determined and the motion is calculated from an explicit numerical integration of its equations of motion. This method has become successful for simulating phenomena such as rock falls and debris flows considering soil as a discrete granular assembly. The Extended Distinct Element Method (EDEM), which is a development of the original DEM, can simulate the behavior of a medium from a continuous state to a discontinuous state following the total fracture process. Iwashita and Hakuno (1990) extended conventional DEM by introducing *pore-springs* between the elements to incorporate continuity due to the effects of pore materials and named this new method the Modified Distinct Element Method (MDEM). The term Extended Distinct Element Method (EDEM) is also used synonymously. The Rigid-body-spring-Model (RBSM) of Kawai T., which is similar to the EDEM, is based on continuum methods such as the finite element method, and the discontinuity across elements are predefined and there cannot be separation between the elements. Moreover, new contact between elements which were not in contact with each other before cannot be modeled as well.

The idea of introducing pore-springs has considerably widened the application area of the conventional DEM because it can model a nonlinearity of a medium automatically: when the pore springs are intact, the model behaves as a continuous medium but when they are destroyed it gradually loses continuity and finally behaves like a perfect discrete medium. Therefore, a series of analyses from a continuous stage to a discontinuous stage can be made and this method can be easily applied to simulate discontinuous and nonlinear phenomena in which every element separates and moves widely after destruction of pore-springs. During the analysis, a new stress field is created by new contacts between elements. They used this method to simulate various geotechnical problems including cliff collapse. Meguro and Hakuno(1988,1990) further developed some aspects of the MDEM and broadened the application area by using it to simulate the fracture of concrete structures.

2.1 Numerical Modeling by the EDEM

For analyzing a large problem, it is quite natural—due to limitations of the computer memory—that every element in a granular assembly can not be assigned different values of parameters. Thus a model is suitably divided into several parts and each part is assigned a set of material parameters. After establishing the element type, *NTP*, of each division, the material parameters of the *NTP* are assigned to the corresponding division.

2.2 *Estimation of the Forces Acting on an Element*

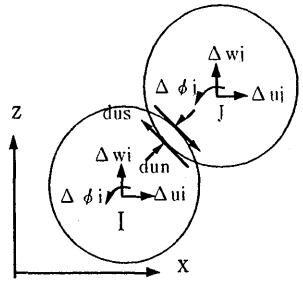

Figure 2.2.1 Elements *i* and *j* with the associated displacements during a small time interval Δt

Two elements, i and j, are shown in Figure 2.2.1. For the element i, Δu_i is the displacement increment in x-direction, Δw_i that in the z-direction, and $\Delta \phi_i$ is its incremental rotation during a small time interval Δt. Similarly, Δu_j, Δw_j, and $\Delta \phi_j$ represent the respective quantities for element j. In Figure 2.2.2, we have the case when element i with radius r_i approaches element j with radius r_j.

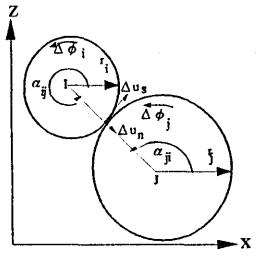

Figure 2.2.2 Elements *i* and *j* at contact

The condition of separation is

$$R_{ij} > r_i + r_j, \tag{2.2.1}$$

where

$$R_{ij} = [(xi-xj)^2 + (zi-zj)^2]^{1/2}, \tag{2.2.2}$$

is the distance between the centers of elements i and j. From Figure 2.2.2, it also follows that, at any time t,

$$\sin \alpha_{ij} = -(z_i-z_j)/R_{ij}, \qquad \cos \alpha_{ij} = -(x_i-x_j)/R_{ij}, \tag{2.2.3}$$

where the angle α_{ij} is taken to be positive when counterclockwise. Then the relative displacement increments in the normal direction Δu_n (approach is considered positive), and in the tangential direction Δu_s (positive when counterclockwise) during Δt between

the two contacting elements i and j can be calculated from the following equations.

$$\Delta u_n = (\Delta u_i - \Delta u_j)\cos\alpha_{ij} + (\Delta w_i - \Delta w_j)\sin\alpha_{ij}, \quad (2.2.4a)$$

$$\Delta u_s = -(\Delta u_i - \Delta u_j)\sin\alpha_{ij} + (\Delta w_i - \Delta w_j)\cos\alpha_{ij} + (r_i\Delta\phi_i + r_j\Delta\phi_j). \quad (2.2.4b)$$

2.2.1 Evaluation of the Contact Forces Between Elements

As shown in Figure 2.2.3, the contact force between elements i and j is resolved into two components on the contact plane—a compressional force f_n in the normal direction and a shear force f_s in the tangential direction.

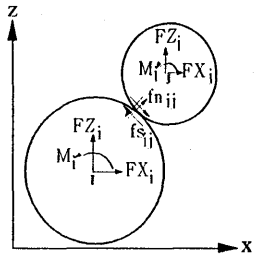

Figure 2.2.3 Forces on the contacting plane

2.2.1.1 Force in Normal Direction

Assuming a parallel disposition of an elastic spring with spring constant k_n and a dashpot with constant c_n respectively as shown in Figure 2.2.4, forces proportional to the relative displacement Δu_n and the relative velocity $\Delta u_n/\Delta t$ during a small time Δt are

$$\Delta f_{en} = k_n \Delta u_n, \quad (2.2.5a)$$

and

$$\Delta f_{dn} = c_n \Delta u_n/\Delta t, \quad (2.2.5b)$$

where the forces are positive in compression.

Thus the elastic reaction force $f_{en,t+\Delta t}$ and the viscous reaction force $f_{dn,t+\Delta t}$ acting in the normal direction at time $t+\Delta t$ are obtained as shown below.

$$f_{en,t+\Delta t} = f_{en,t} + \Delta f_{en} \quad (2.2.6a)$$

$$f_{dn,t+\Delta t} = f_{dn,t} + \Delta f_{dn}. \quad (2.2.6b)$$

In the case of the conventional DEM, tensile force could not be considered and the additional condition given below was attached to equations (2.2.6), i.e., $f_{en,t} < 0$ implies that

$$f_{en,t} = 0, \quad (2.2.7a)$$

$$f_{dn,t} = 0. \quad (2.2.7b)$$

Then the force (compression) in the normal direction between two elements at a time t is

calculated as

$$f_{n,t} = f_{en,t} + f_{dn,t} \cdot \quad (2.2.8)$$

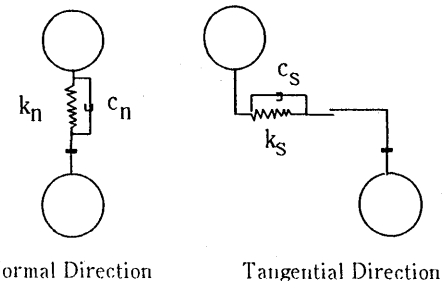

Figure 2.2.4 Element springs in normal and tangential directions (DEM Modeling)

2.2.1.2 Force in Tangential Direction

Assuming a parallel disposition of an elastic spring with spring constant k_s and a dashpot with constant c_s respectively as shown in Figure 2.2.4, forces proportional to the relative displacement Δu_s and the relative velocity $\Delta u_s/\Delta t$ during a small time Δt are

$$\Delta f_{es} = k_s \Delta u_s , \quad (2.2.9a)$$

and

$$\Delta f_{ds} = c_s \Delta u_s/\Delta t. \quad (2.2.9b)$$

Hence, the elastic reaction force $f_{es,t+\Delta t}$ and the viscous reaction force $f_{ds,t+\Delta t}$ acting in the normal direction at time $t+\Delta t$ are obtained as shown below.

$$f_{es,t+\Delta t} = f_{es,t} + \Delta f_{es} \quad (2.2.10a)$$

$$f_{ds,t+\Delta t} = f_{ds,t} + \Delta f_{ds} \quad (2.2.10b)$$

Here, two conditions have been added; if $f_{en,t} < 0$ then

$$f_{es,t} = f_{ds,t} = 0, \quad (2.2.11a)$$

and if $|f_{es,t}| > \mu f_{en,t}$, then

$$f_{es,t} = \mu f_{en,t} .SIGN(f_{es,t}), \quad (2.2.11b)$$

$$f_{ds,t} = 0, \quad (2.2.11c)$$

where μ is the coefficient of friction.

The above conditions indicate that shear deformation is due to the friction force between elements near the contacting point. Equation (2.2.11a) corresponds to the no contact condition and equations (2.2.11b) and (2.2.11c) show the limitations of the friction force. The shear force at time t between two elements in the tangential direction, $f_{s,t}$, is obtained as

$$f_{s,t} = f_{es,t} + f_{ds,t} \cdot \quad (2.2.12)$$

2.2.2 Summation of the Forces Acting on an Element

Once we obtain the contacting forces $f_{n,t}$ and $f_{s,t}$ using the above equations, for all elements j that are in contact with the element i, we can calculate the resultant forces FX_i and FZ_i in both x- and z-coordinate directions, and a moment M_i at the center (the moment being taken as positive when counterclockwise) as follows

$$FX_{i,t} = \Sigma_j \{-f_{n,t} \cos\alpha_{ij} - f_{s,t} \sin\alpha_{ij}\}, \quad (2.2.13a)$$

$$FZ_{i,t} = \Sigma_j \{-f_{n,t} \sin\alpha_{ij} + f_{s,t} \cos\alpha_{ij}\} - m_i \cdot g, \quad (2.2.13b)$$

$$M_{i,t} = r_i \cdot \Sigma_j f_{s,t}, \quad (2.2.13c)$$

where,

$$j=1,nke(i). \quad (2.2.13d)$$

The array *nke(i)* has all elements in contact with the element i, m_i is the mass of the element i and g is the acceleration due to gravity.

2.3 Numerical Integration of Equations of Motion

By knowing the forces acting, we can very easily find the accelerations at time t from Newton's second law as

$$(d^2u_i/dt^2)_t = FX_{i,t}/m_i, \quad (2.3.1a)$$

$$(d^2w_i/dt^2)_t = FZ_{i,t}/m_i, \quad (2.3.1b)$$

$$(d^2\phi_i/dt^2)_t = M_{i,t}/I_i, \quad (2.3.1c)$$

where I_i is the moment of inertia of the element i. If ρ is the mass per unit area, we have

$$m_i = \rho \pi r_i^2, \quad (2.3.2a)$$

$$I_i = 1/2 \cdot \rho \pi r_i^4. \quad (2.3.2b)$$

By explicitly integrating the equations (2.3.1), we obtain velocities at time t as follows.

$$(du_i/dt)_t = (du_i/dt)_{t-\Delta t} + (d^2u_i/dt^2)_t \cdot \Delta t \quad (2.3.3a)$$

$$(dw_i/dt)_t = (dw_i/dt)_{t-\Delta t} + (d^2w_i/dt^2)_t \cdot \Delta t \quad (2.3.3b)$$

$$(d\phi_i/dt)_t = (d\phi_i/dt)_{t-\Delta t} + (d^2\phi_i/dt^2)_t \cdot \Delta t \quad (2.3.3c)$$

Here, integrating with respect to time again, we obtain the displacement increments at time t as shown below.

$$\Delta u_{i,t} = 1/2 \{(du_i/dt)_{t-\Delta t} + (du_i/dt)_t\} \cdot \Delta t \quad (2.3.4a)$$

$$\Delta w_{i,t} = 1/2 \{(dw_i/dt)_{t-\Delta t} + (dw_i/dt)_t\} \cdot \Delta t \quad (2.3.4b)$$

$$\Delta \phi_{i,t} = 1/2 \{(d\phi_i/dt)_{t-\Delta t} + (d\phi_i/dt)_t\} \cdot \Delta t \quad (2.3.4c)$$

These new values of displacement increments are used in the force-displacement law and the cycle is repeated from equations (2.2.4) through equations (2.3.4), for the next time station $t+\Delta t$. Thus it is seen that the calculations performed in the DEM are cycling through a force-displacement law and the law of motion. The force-displacement

law is applied at each contact point of an element with another element and the contact forces in the normal and tangential directions are determined to yield the resultant force acting on that element. When this has been accomplished for every element in the assembly, new accelerations are calculated from the law of motion and subsequently the velocities and the incremental displacements are obtained through an explicit numerical integration of equations of motion. The new co-ordinates of the elements are updated as

$$x_{i,t} = x_{i,t-\Delta t} + \Delta u_{i,t}, \tag{2.3.5a}$$

$$z_{i,t} = z_{i,t-\Delta t} + \Delta w_{i,t}, \tag{2.3.5b}$$

and

$$\phi_{i,t} = \phi_{i,t-\Delta t} + \Delta \phi_{i,t}. \tag{2.3.5c}$$

2.4 DEM with Pore-Springs

Additional springs, termed *pore-springs,* were introduced to the conventional DEM by Hakuno, Iwashita and Meguro to simulate continuity during the analysis. The purpose was to conduct fracture simulations from a continuous state to a discontinuous state following the total fracture process.

2.4.1 Criterion for Setting a Pore-Spring

Additional springs (*pore-springs*) are introduced between elements in both normal and tangential directions as shown in figure 2.0.1. To divide the model, pore-springs are set between elements i and j that fall in division $n1$ of the model with element types $NTYPE(i) = NTYPE(j) = n1$. Input parameters for elements belonging to each of these divisions of the model—which may be different from one division to the other—are decided before the numerical experiment. The criterion for setting pore-springs between elements i and j at the initial stage is

$$R^{o}_{ij} \leqq \alpha(n1) \cdot (r_i + r_j), \tag{2.4.1}$$

where r_i and r_j are radii of the elements i and j, and R^{o}_{ij} is the initial distance between their centers given by

$$R^{o}_{ij} = [(x_{io}-x_{jo})^2 + (z_{io}-z_{jo})^2]^{1/2}, \tag{2.4.2}$$

and α is some value of the parameter for establishing pore-springs between elements falling in the division $n1$. It is clear that for $\alpha(n1) \leqq 1$, there will be no pore-springs between elements belonging to this division. The length of the pore-spring, L_{ij}, is taken as the initial distance between the elements i and j according to

$$L_{ij} = R^{o}_{ij}, \tag{2.4.3}$$

and memorized for later use.

2.4.2 Fracture criteria for the Pore-Springs

First, the pore material between the particles is firmly and stably associated with

them. But when an external force acts on the model, the elements begin to move and cracks are produced in the pore material by tension or shear force. Because of these cracks, the pore material loses its tensile resistance and can withstand only compression, and the shear deformation is resisted by the pore-spring only when there is a compressive normal force acting between the elements. On the basis of these assumptions, the fracture process of pore-springs has been divided into two states: ① The pore-spring is intact. It resists not only compression but also tension and shearing deformation, when external compressive or tensile force acts on it; ② Cracks are produced in the pore material. The pore-spring is only effective for transmitting compressive force between the elements. The pore-spring has no tensile resistance. It resists shear when there is a compressive force acting between the elements.

In the EDEM, there are two conditions under which the state of a pore-spring changes from first to second: ① when the pore-spring is fractured by tensile force in the normal direction, and ② when the pore-spring is fractured by shear force in the tangential direction. During the calculations, the above conditions are noted and memorized. At the beginning, all the pore-springs belong to state 1, and the conditions 1 and 2 result from the following criteria.

2.4.2.1 Fracture Criteria in Normal Direction

A critical strain in the pore-spring is specified in the normal direction. The pore-spring changes from the first to the second state when the strain in it at time t satisfies the inequality

$$R^{0}_{ij,t} = \beta(n1) \cdot L_{ij} \ , \qquad (2.4.4)$$

in which $R^{0}_{ij,t}$ is the distance between centers of the elements i and j at time t; L_{ij} is the initial distance between the elements as given in the equation (2.4.3) and $\beta(n1)$ is a critical strain specified for the division $n1$.

Although these criteria show that pore-spring destruction is caused by tensile strain in the normal direction, pore-springs in both the normal and tangential directions are assumed to change from state 1 to state 2. At the same time, the cause of the pore-spring destruction is memorized as tensile strain in the normal direction.

2.4.2.2 Fracture Criteria in Shear Direction

The shear force acting between elements cannot exceed the shear strength τ_c given by the Coulomb's equation

$$\tau_c = C + \mu F_n, \qquad (2.4.5)$$

where C is the cohesive force (constant), μ the friction coefficient and F_n the normal force acting between elements i and j. When the force acting tangentially on the pore-spring is larger than τ given by equation (2.4.5), the states of the pore-spring in both the normal and the tangential directions are assumed to change from state 1 to state 2 and the cause of destruction of the pore-spring is memorized as being shear, and the force acting tangentially on the pore-spring becomes τ_c.

2.5 Contribution from the Pore-Springs to the Total force

The forces given by equations (2.2.8) and (2.2.12), and the forces due to pore-springs between elements—presented below—are summed up to find the total force acting on an element.

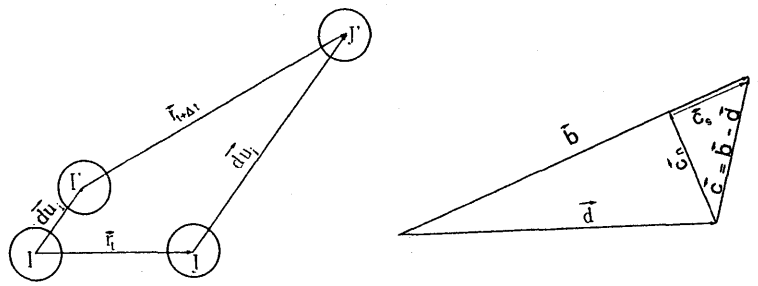

(a) Displacements during Δt (b) Vector representation of the relative positions

Figure 2.5.1 Force contribution from the pore-springs (EDEM Modeling)

From the vector diagram in Figure 2.5.1(b),

$$\mathbf{c}_n = \{ |\mathbf{b}| - |\mathbf{d}| \} \cdot \mathbf{b}/|\mathbf{b}|, \tag{2.5.1}$$

$$\mathbf{c}_s = \mathbf{c} - \mathbf{c}_n, \tag{2.5.2}$$

$$\mathbf{c'}_s = \{|\mathbf{c}_s| - r_i\phi_i - r_j\phi_j\}.\mathbf{c}_s/|\mathbf{c}_s|, \tag{2.5.3}$$

where c'_s is the total shear displacement including the contribution of rotation of elements i and j and the bold letters denote vector quantities. In the above equations, ϕ_i and ϕ_j are angles made by the position vectors of elements i and j respectively. If the forces from the pore-springs in the normal and the tangential directions are represented by f_{pn} and f_{ps}, we have

$$\mathbf{f}_{pn} = k_{pn}\mathbf{c}_n, \tag{2.5.4}$$

$$\mathbf{f}_{ps} = k_{ps}\mathbf{c'}_s, \tag{2.5.5}$$

where k_{pn} and k_{ps} are pore-spring constants in the normal and shear directions respectively. When $|b| < |d|$, a compressive force acts in the pore-spring in the normal direction and we have from the Coulomb's law

$$|\mathbf{f}_{ps}| \leqq C + |\mathbf{f}_{pn}| \cdot \tan\phi, \tag{2.5.6}$$

and when there is tension in the pore-spring, we have

$$|\mathbf{f}_{ps}| \leqq C, \tag{2.5.7}$$

meaning that the shear force in the pore-spring can not exceed the cohesive force C.

3. Parameters of Simulation using the EDEM

Parameters of the simulation using the EDEM include spring constants of the interacting elements, constants for setting pore-springs between neighboring elements and constants for the defined criteria for the destruction of these springs, cohesion and the coefficient of friction, among others.

constants for the defined criteria for the destruction of these springs, cohesion and the coefficient of friction, among others.

3.1 Determination of the Spring and Damping Constants

The spring constants in the normal and tangential directions are based on the one-dimensional wave propagation equation

$$\partial^2 Y/\partial t^2 = V^2 \partial^2 Y/\partial x^2, \tag{3.1.1}$$

where V is the wave propagation speed in the objective medium. For brevity, the expressions for the composite elastic constants KN and KS determined from the wave speeds V_p and V_s are given below. For details, the reader is referred to Rimal (1992).

$$KN = 1/4\ \pi\ \rho\ V_p^2 \tag{3.1.2a}$$

$$KS = 1/4\ \pi\ \rho\ V_s^2 \tag{3.1.2b}$$

From these composite spring constants in the normal and tangential directions, element spring constants k_{en} and k_{es}, and pore-spring constants k_{pn} and k_{ps} are calculated as shown in the Equations (3.1.4). This is done by dividing the composite constants into pore part and element part in the ratios s_n :1 and s_s:1 in the normal and tangential directions respectively as shown in equations (3.3).

$$k_{pn} = s_n k_{en} \tag{3.1.3a}$$

$$k_{ps} = s_s k_{es} \tag{3.1.3b}$$

where

$$0 \leqq s_n \leqq 1 \tag{3.1.3c}$$

and

$$0 \leqq s_s \leqq 1. \tag{3.1.3d}$$

Thus the individual spring constants of the EDEM are computed as follows.

$$k_{en} = 1/(1+s_n) \cdot KN = \pi\ \rho\ V_p^2/\{4(1+s_n)\} \tag{3. 1.4a}$$

$$k_{pn} = s_n/(1+s_n) \cdot KN = \pi\ \rho\ V_p^2 s_n/\{4(1+s_n)\} \tag{3. 1.4b}$$

$$k_{es} = 1/(1+s_s) \cdot KS = \pi\ \rho\ V_s^2/\{4(1+s_s)\} \tag{3. 1.4c}$$

$$k_{ps} = s_s/(1+s_s) \cdot KS = \pi\ \rho\ V_s^2 s_s/\{4(1+s_s)\} \tag{3. 1.4d}$$

Considering a parallel disposition of viscous dashpot in each direction, the coefficients of damping c_n and c_s in the normal and tangential directions can be written as follows.

$$c_n = 2\ \xi_n\ (m \cdot KN)^{1/2} \tag{3.1.5a}$$

$$c_s = 2\ \xi_s\ (m \cdot KS)^{1/2} \tag{3.1.5b}$$

From the equations (3.1.4) and (3.1.5), we thus arrive at the damping constants as

$$c_{en} = 2\ \xi_{en}\ (m \cdot k_{en})^{1/2}, \tag{3.1.6a}$$

$$c_{es} = 2\ \xi_{es}\ (m \cdot k_{es})^{1/2}, \tag{3.1.6b}$$

$$c_{pn} = 2\xi_{en}(m \cdot k_{pn})^{1/2}, \quad (3.1.6c)$$

$$c_{ps} = 2\xi_{es}(m \cdot k_{ps})^{1/2}, \quad (3.1.6d)$$

where ξ denotes the damping ratio in the direction given by the subscripts associated with it in the above equations.

3.2 Determination of the Parameters C_{EDEM} and μ

At the contact plane of two neighboring elements, the shear stress cannot exceed the strength given by Coulomb's law. The cohesive force given by the constant C_{EDEM} is determined from the configuration of the elements in an assembly. Figure 3.2.1 shows the flow of the procedure to determine the constant C_{EDEM}.

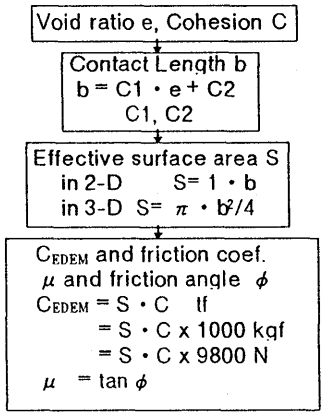

Figure 3.2.1 Flow of determination of C_{EDEM}

The Mohr-Coulomb's equation is

$$\tau = C + \sigma \tan\phi. \quad (3.2.1)$$

If s is the effective contact area in the contact region of two elements as noted in the flow chart of the Figure 3.2.1, the critical shear force FS_{crit} acting between the elements can be written as

$$FS_{crit} = \tau_c s = s C + s \sigma \tan\phi. \quad (3.2.2)$$

Similarly, the normal force over an area s simply becomes

$$F_n = s\sigma. \quad (3.2.3)$$

Combining equations (3.2.2) and (3.2.3) then gives the relation between normal and the shear force as

$$FS_{crit} = s C + F_n \tan\phi. \quad (3.2.4)$$

In the EDEM using the friction coefficient μ, if C_{EDEM} represents the cohesive force, the above equation becomes

$$FS_{crit} = C_{EDEM} + F_n \cdot \mu, \quad (3.2.5)$$

where $C_{EDEM} = s \cdot C$ and $\mu = tan\,\phi$. In the two-dimensional case, the area $s = b \cdot 1$, and $C_{EDEM} = b \cdot C$, where the constant b depends upon the arrangement of elements inside a granular assembly. Figure 3.2.2 shows different configurations of the element assembly and the corresponding values of the constant b.

Figure 3.2.3 shows the relationship between void ratio and the contact length, and three points corresponding to the three dispositions are also shown. From figures 3.2.2 and 3.2.3, we can determine the parameter b for a void ratio e of the model and then determine the cohesive force C_{EDEM}.

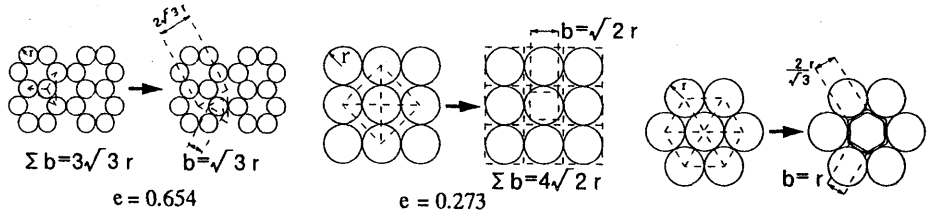

Figure 3.2.2 Different configurations of element assembly and the corresponding values of the constant b

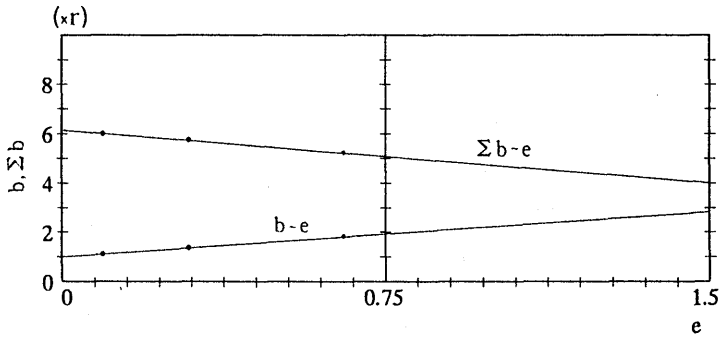

Figure 3.2.3 Relationship between void ratio and contact length

3.3 Determining Integration Time-step Δt

The time-step for integrating the equations of motion of every element in an assembly should be chosen in such a way that the displacement wave can propagate over the smallest element present in the objective medium, i.e.,

$$\Delta t \leqq D_{min} / V, \qquad (3.3.1)$$

where V is the velocity of wave propagation in the objective medium and D_{min} is the diameter of the smallest element in an assembly. Considering problems resulting from the numerical instability, a smaller time-step than the one computed from the above inequality is taken.

4. Computer Simulation of Fracture and Associated Phenomena

4.1 General

Various researchers have studied the fracture behavior of both artificial and natural rock specimens (Mogi, 1962,1963,1967,1968), foam-rubber models of earthquake fault (Brune et al., 1973), glass plate (Savage et al.,1963) and wooden board (Kishinouye, 1937) by conducting experiments under controlled conditions in a laboratory. Their purpose was to better understand the fracturing of the Earth's crust, by making inferences from the results of such studies. Dilatation, which is believed to occur from the progressive development of cracks inside the Earth's crust, and merger of these cracks leading to the formation of a fault are some of the important topics discussed in such studies.

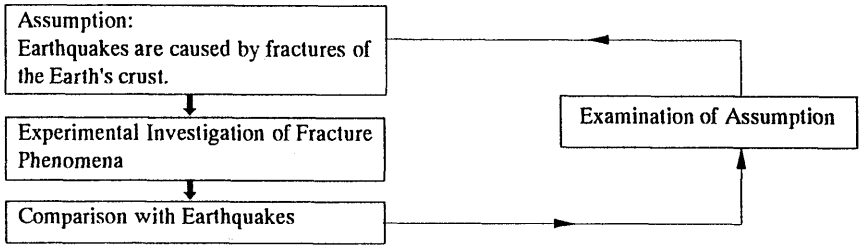

Figure 4.1.1 Fracture theory of Earthquakes (after Mogi, 1967)

Figure 4.1.1 shows the assumptions for the fracture theory of earthquakes, after Mogi. He conducted experiments on both artificial and natural rock specimens in the laboratory and based on the geometrical structure of the specimens tested, he classified the different types of sequences of crack occurrences and compared them to the real earthquake sequences.

It is obvious, however, that many difficulties such as altering the boundary conditions for simulations, high cost of repeated tests, etc., arise when conducting experiments on rock specimens. The Extended Distinct Element Method (EDEM), as explained in section 2, has the strong advantage in that it can be used to simulate the behavior of a medium from a continuous stage to a discontinuous stage following the total fracture process. Moreover, because it is a numerical method, simulation parameters as well as boundary conditions can be handled with ease, enabling one to study different phenomena relatively easily. Hence, the study of fracture phenomena of the Earth's crust can be thought to be a potential field in terms of its applications. The EDEM is used in this and the following sections to study phenomena concerning the fracture of the Earth's crust. Progressive development of cracks, dilatation, stick-slip-type of forces and Acoustic Emission (A.E.) of the EDEM models are the subjects of discussion. The importance of studying these phenomena lies in the fact that they are believed to be very closely related to the occurrence of earthquakes.

4.2 Model Development

In preparing the model used in this study, 1,800 elements with their radii following a log-normal distribution are generated (see Rimal (1992), for details) in a

region having dimensions of 400m by 200m (see Figure 4.2.1).

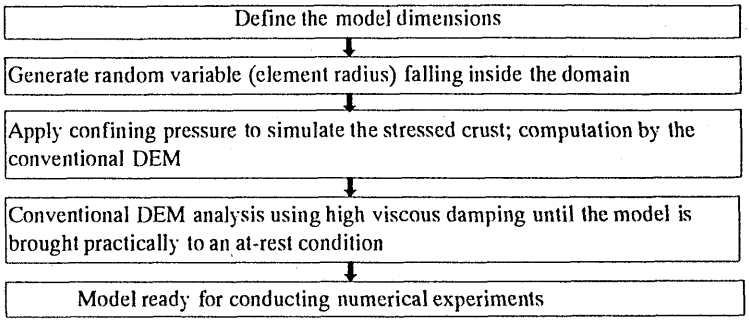

Figure 4.2.1 A simplified Flow of the Model Preparation

Table 4.2.1 Description of geometry of the model

Model Size	400m x 200m	Number of inside elements	1800
Maximum Element-Size	12.5m	Number of boundary wall elements	240
Minimum Element-Size	5.0m	Number of outer frame elements	166
Size of boundary wall elements	5.0m	Total number of elements	2206

Table 4.2.2 Parameters used for the fracture simulation by EDEM

	Normal Direction			Shear Direction	
Element	Spring Constant ken (N/m)	9.0×10^{8}	Element	Spring Constant kes (N/m)	3.0×10^{8}
	Damping Constant cen (Ns/m)	2.0×10^{6}		Damping Constant ces (Ns/m)	1.2×10^{6}
Pore	Spring Constant kpn (N/m)	9.0×10^{7}	Pore	Spring Constant kps (N/m)	3.0×10^{7}
	Damping Constant cpn (Ns/m)	0.0		Damping Constant cps (Ns/m)	0.0
	Critical value α for setting pore spring	1.1		Critical value β for fracture of pore spring	1.1

To get a closely packed assembly, and to simulate the initially existing stress near the region of an earthquake fault, the model is pressed from all sides and the computation is done by the conventional DEM. Figure 4.2.1 shows the flow of model preparation. The parameters for the analysis using DEM are listed in Tables 4.2.1 and 4.2.2.

Spring constants of the elements in normal and tangential directions are determined from the assumed wave propagation velocities V_p and V_s respectively in the objective medium. The method of determination of these parameters has been explained in section 3. It is usual, in the DEM, to consider a sample in which the velocities are reduced

to practically zero, as a stable sample. This stage is reached by applying viscous damping to all the elements in a granular assembly. Figure 4.2.2 shows the model after following the steps outlined in Figure 4.2.1.

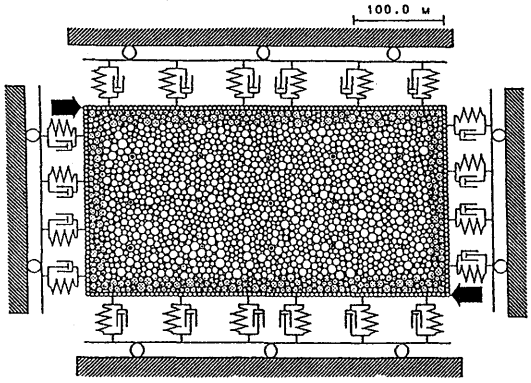

Figure 4.2.2 Model prepared by packing 1,800 circular elements. The inside-element radius is a random variable following the log-normal distribution and the 240 supporting wall elements are of equal size (radius = 2.5m). The supporting walls are allowed to deflect under a displacement-proportional restoring force.

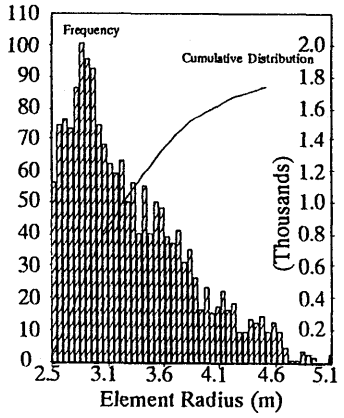

Figure 4.2.3 Distribution of Element Radius in the Model (Element Radius is a random variable following the lognormal distribution)

Figure 4.2.3 shows the distribution of element radius generated with a mean μ = 3.5 and a standard deviation σ = 1.0, which enter into the equations 4.2.1. Figure 4.2.4 shows the initial distribution of pore-springs. The pore-springs are set in the beginning of the simulation. Destruction of a pore-spring gives rise to the appearance of a crack inside the model.

$$\lambda = \ln \mu - 1/2\ \zeta^2 \qquad (4.2.1a)$$

$$\zeta^2 = \ln (1 + \sigma^2/\mu^2) \qquad (4.2.1b)$$

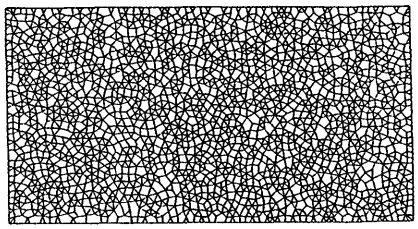

Figure 4.2.4 Distribution of pore-springs, set between the circular elements in the model, after being packed using the conventional DEM. Breaking of a pore-spring gives rise to the occurrence of a crack in the EDEM modeling. Thus, progressive development of cracks can be simulated automatically.

4.3 Shearing the Models with Displacement Control

The sides of the model are displaced in the direction of the arrows shown in Figure 4.2.2. The top, bottom and the side walls are supported on springs, which allow them to move under the influence of incremental forces over the existing confining forces. Parameters used for the simulation are noted in Table 4.2.2. The purpose of this test is to study the stick-slip behavior of the reaction force, the dilatation phenomenon and the acoustic emission (AE) characteristics of a randomly heterogeneous medium, for the first time, by a numerical experiment. Because it is not possible to study the progressive development of cracks inside a medium by other numerical methods, this may be regarded as a relative merit and, therefore, has been emphasized in this study.

Figures 4.3.1 and 4.3.2 respectively show distributions of the displacement vectors and the progressive development of cracks in the model. As is evident from the figure, cracks align to one of the diagonal directions and this analysis naturally simulates the growth of cracks and their merger. Figure 4.3.3 shows the distribution of the sum of the total boundary forces of one half of the model, in both X- and Z-directions, during the experiment and it is seen that the forces rise and drop showing a stick-slip type of behavior. Figure 4.3.4 shows dilatation of the model. As can be seen from the figure, the area first decreases and then increases (dilatation); this is reported to be true also in the case of experiments with rock specimens, in the field of rock mechanics (see Brace and Byerlee, 1966; Brune, 1973; Stuart, 1974). The progressive development of cracks obtained in this manner is a very strong advantage of the EDEM.

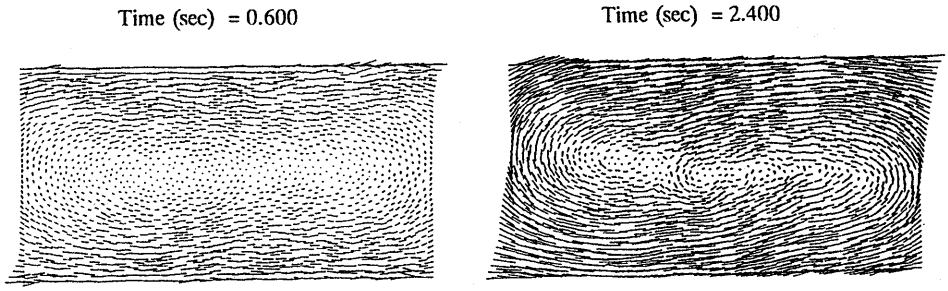

Figure 4.3.1 Distribution of displacement vectors in the model at selected time stations.

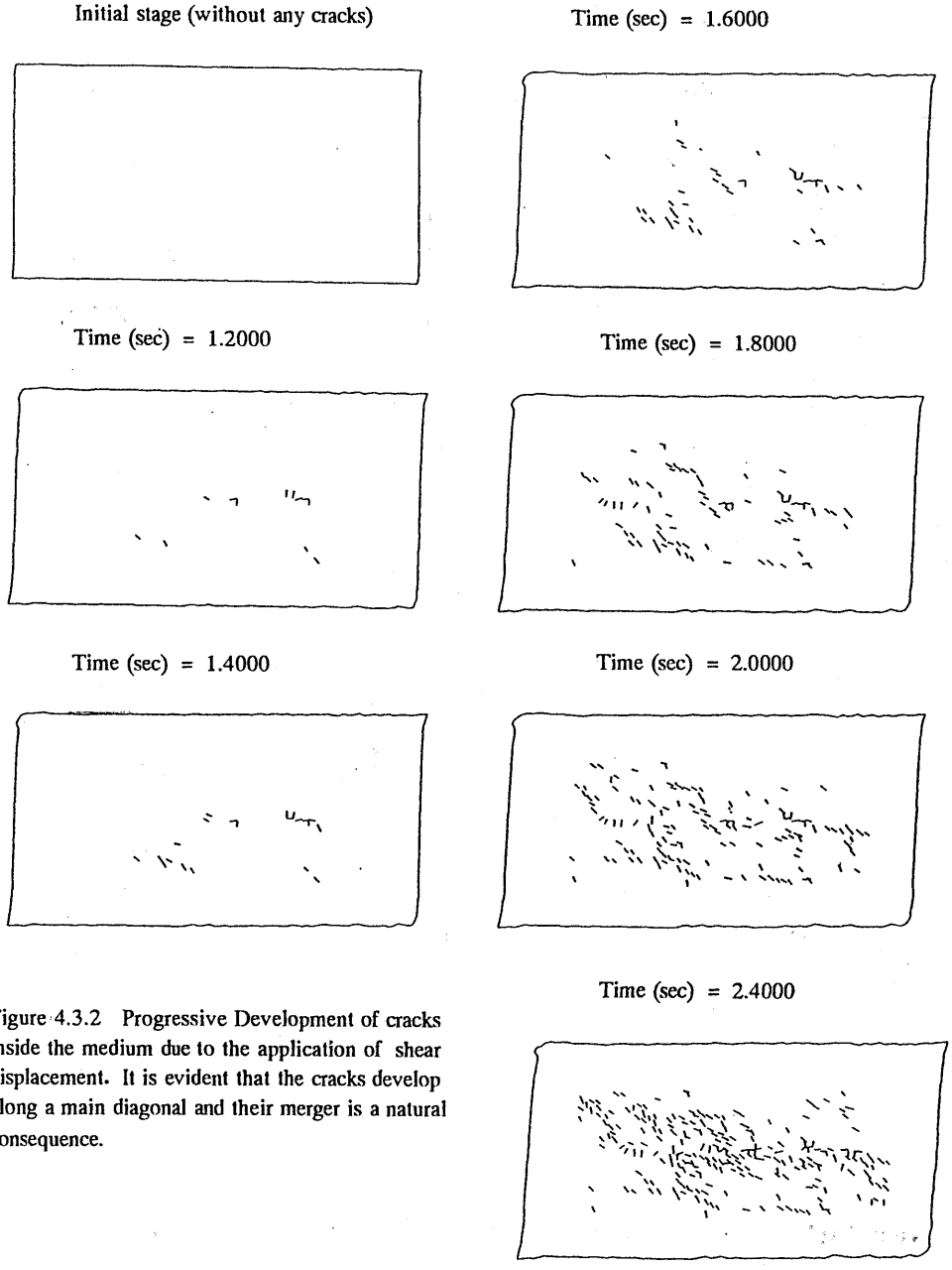

Figure 4.3.2 Progressive Development of cracks inside the medium due to the application of shear displacement. It is evident that the cracks develop along a main diagonal and their merger is a natural consequence.

Figure 4.3.5 shows a plot of the frequency of cracks versus time of occurrence. Also shown in Figure 4.3.6 is a plot of the frequency distribution of an earthquake swarm (after Kishinoue, 1935) for a qualitative comparison. The heterogeneous nature of the EDEM model—due to random size of elements employed in the simulation—may be attributed for the observed similarity.

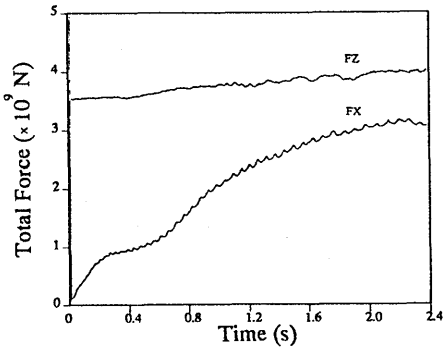

Figure 4.3.3 Distribution of the sum of forces FX and FZ of one half of the model

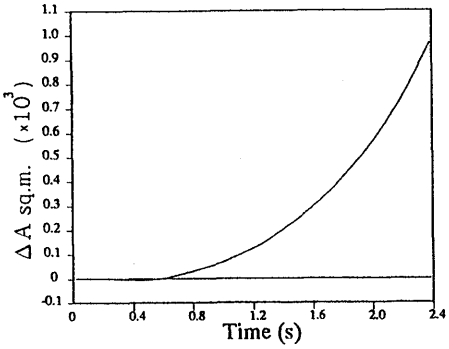

Figure 4.3.4 Dilatation of the model

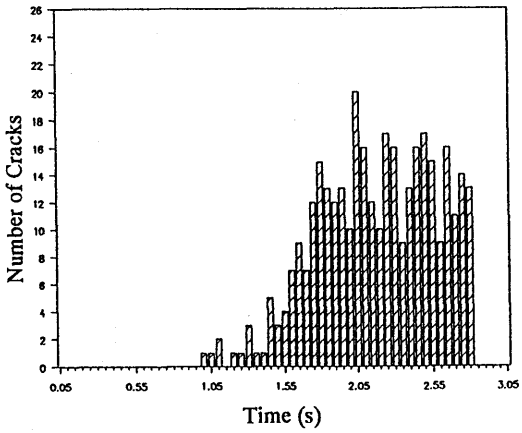

Figure 4.3.5 Frequency of crack occurrences inside the model

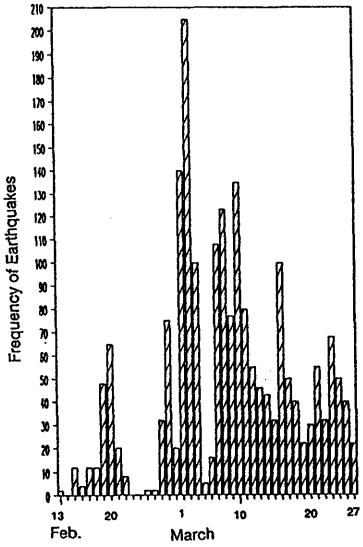

Figure 4.3.6 Frequency distribution of swarm type of earthquakes (Ito earthquake of 1934, after Kishinoue, 1937)

5.Near Field Characteristics Studied From a Pre-strained Model

5.1 General

Researchers in various fields of science, including civil engineers, are interested in studying the effects of high-frequency components of earthquake motions. The mechanism of generation of high-frequency ground motion is studied by various researchers (e.g. Das and Aki, 1977). Mikumo and Miyatake (1987) used the finite

difference method and Toki et al. (1985) applied the finite element method to study the earthquake source process. The weak point of the finite difference method is that the grid points cannot move in space, so a large and finite displacement due to rupture cannot be modeled. In the case of the finite element method, attaching a node to another previously unconnected node—due to large displacement—cannot be done easily. The Extended Distinct Element Method (EDEM) has a very strong advantage by which it can simulate the behavior of a model from a continuous stage to a discontinuous stage following the total fracture process. The progressive development of cracks inside a model can be obtained in a very natural way. Moreover, unlike the finite difference method, the elements can have large displacements caused by the rupture so that the opposite sides of the fault can fling past each other. A new stress field forms due to new contact between elements which were not in contact before. Recognizing these advantages, the method is used—for the first time—in this study to simulate near-field characteristics of fault rupture.

An earthquake is the result of a sudden relaxation of elastic strains due to a rupture and the accumulation of strain in the Earth's crust before the rupture takes a long time. Therefore, it is not possible to simulate this process unless some plausible assumptions are made. In this section, several steps necessary to simulate a critical state of the crust just prior to rupture are developed and outlined. Fracture is caused by parameterization and the characteristics of displacement near the rupture edge and friction force are observed.

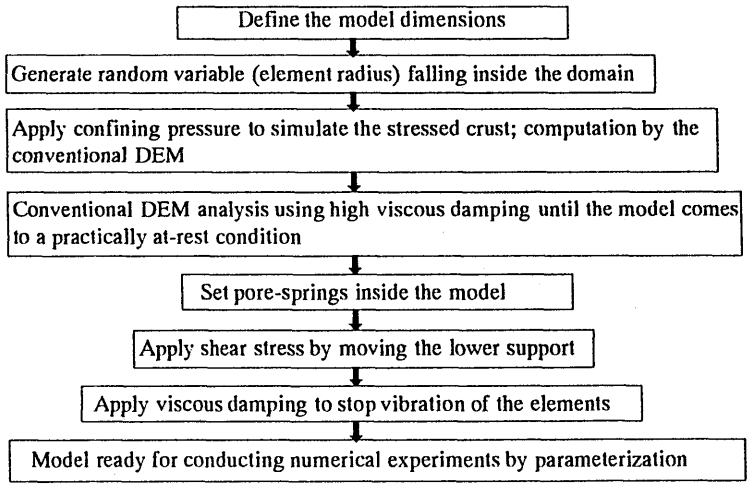

Figure 5.2.1 Flow of model preparation; realization of a stressed crust numerically

5.2 Model Description

A model is prepared following the sequence outlined in Figure 5.2.1. The model's dimensions, geometry, element size and various parameters for simulation are the same as those in section Four. In addition, a measure is taken to numerically simulate a state of high shear stress at the bottom of the model: The lower support of the model, shown in

Figure 5.2.2, is displaced with constant rate shear displacement in the direction of the arrow until a final value of 7.5m, and viscous damping was used for every element inside the model until the model comes practically to an *at-rest* condition, which is checked by plotting the average velocity of all the elements inside the model.

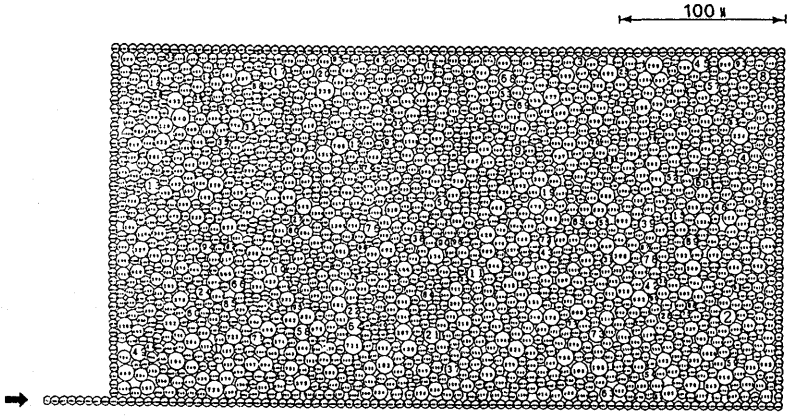

Figure 5.2.2 (a) Distribution of elements inside the model. The model consists of 1,800 inner elements following a log-normal direction of the element size, and 248 outer elements that are of same size.

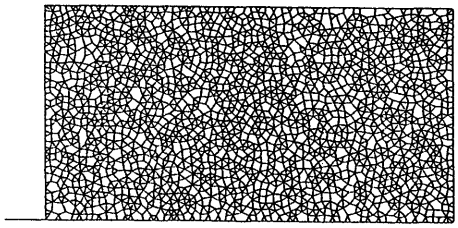

Figure 5.2.2 (b) Pore-spring distribution inside the model used for the study

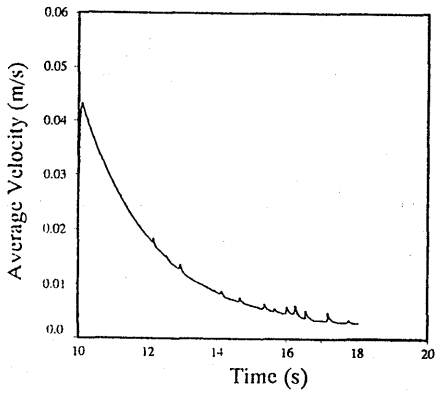

Figure 5.2.3 Average velocity distribution as a check to see whether the model came practically to an *at-rest* condition

Plot of the distribution of average velocities of the elements inside the model in Figure 5.2.3 shows that the model has already reached a practically *at-rest* condition at the end of the time axis where the average velocity is about 4 mm/sec. It is necessary to keep each of the parameters β and c, which control the fracture criteria, at a higher value during application of shear displacement so that no cracks are produced before the real experiment is conducted on the model.

Figure 5.2.4 shows the sum of the forces FX and FZ of elements at the base during application of damping and it is seen that the forces have become almost constant at the end of the time axis.

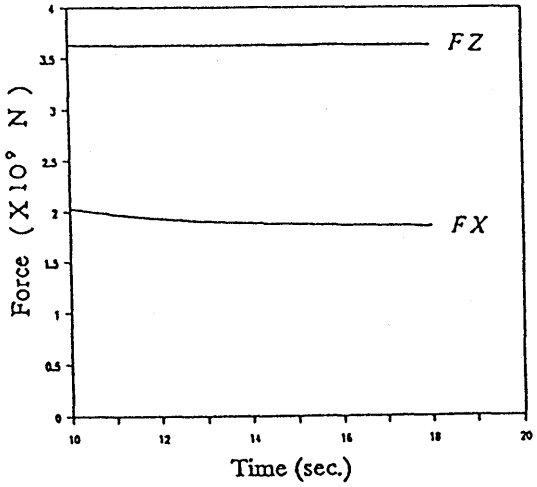

Figure 5.2.4 Sum of the forces FX and FZ of elements at the base during the period of damping to check whether the model came practically to an *at-rest* condition

Figure 5.2.5 shows distribution of elements in the model with the lower support displaced. Numbers 1 through 7 are marked on the top of this figure for plotting the responses of elements lying on these vertical lines.

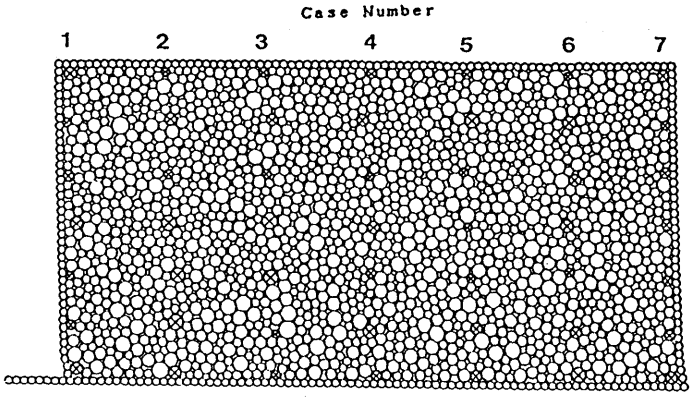

Figure 5.2.5 Distribution of elements inside the model; the lower support has been horizontally displaced to apply a high shear stress and the model is brought to rest by damping. Elements marked by crosses are selected for studying the displacement response.

Critical parameters are determined before starting the numerical experiment by parameterization. To do so, first the parameters β and C_{EDEM} are reduced gradually, as a function of time, in the EDEM analysis without applying any external load. At certain values of each of these parameters the first crack occurs and these values are thus taken as the critical values β_{cr} and $C_{EDEM,cr}$ for the subsequent analyses. By varying the parameters of the EDEM, it is possible to study various fracture phenomena that are difficult to approach by other methods.

5.3 Simulation Results and Discussion

Starting with the model in Figure 5.2.5, the parameter β is gradually reduced so that it changes from β_{cr} to a smaller value. The purposes of this experiment are to study the nature of displacement very near the rupture edge and drop of the shear force at the base of the model brought about by the rupture.

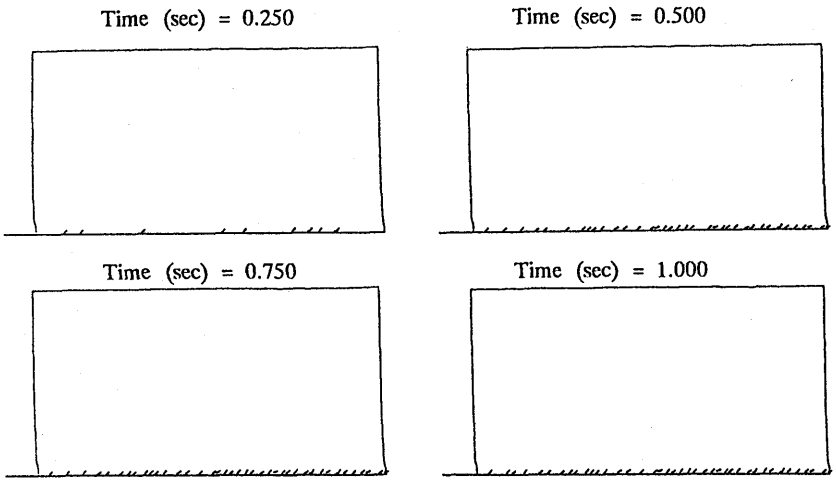

Figure 5.3.1(a) Distribution of cracks at some selected time stations. The cracks were created by parameterization after the steps outlined in Figure 5.2.1.

Figures 5.3.1(a) and (b) respectively show the locations of cracks and the displacement vectors inside the model due to parameterization, at selected times.

Figure 5.3.2 shows the distribution of sum of the force FX of each element lying on the lower support during the rupture. Due to the occurrence of cracks in the highly stressed region, a consequent drop of the sum of force FX (stress drop) is also seen in this figure. It is also clear that the drop of force occurs with a higher frequency at the beginning. This observation is made for the sum of vertical reaction forces, FZ, in Figure 5.3.3 as well. The high frequency may be attributed to the increased fracturing activity (around 0.5 s) when we see the occurrence of cracks in Figure 5.3.1(a).

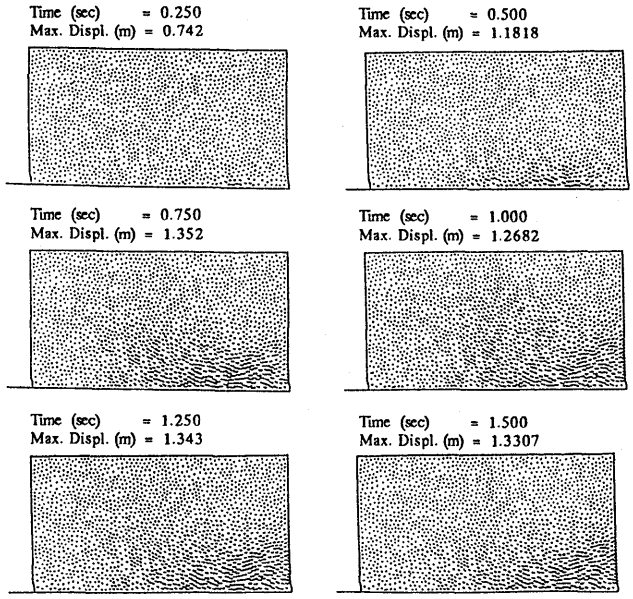

Figure 5.3.1(b) Distribution of displacement vectors at some selected time stations.

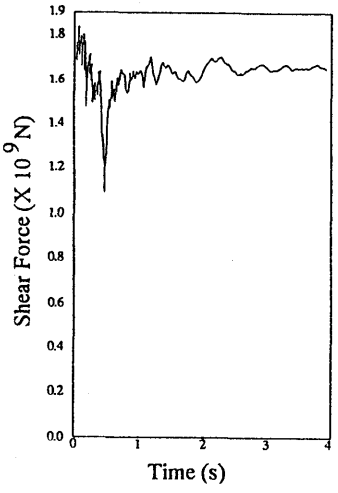

Figure 5.3.2 Nature of total horizontal (shear) force at the base

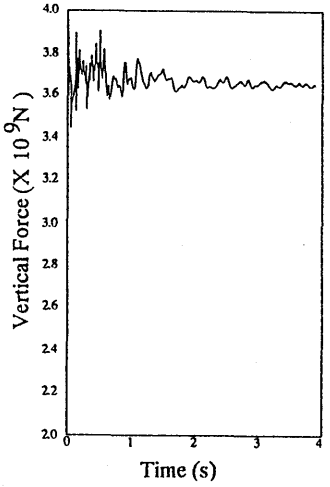

Figure 5.3.3 Nature of total vertical force at the base

Figure 5.3.4 shows the distribution of displacement time-histories of elements marked by crosses inside the model (see Figure 5.2.5). For brevity, the results of only a few cases are presented. Figures 5.3.5, taken from a paper by Brune (1973), shows similar results from tests conducted on foam rubber models of earthquake faults in the laboratory. This type of result is also obtained by the finite element method (see, for example, Toki et al.). In the dislocation theory of earthquakes when using the theoretical

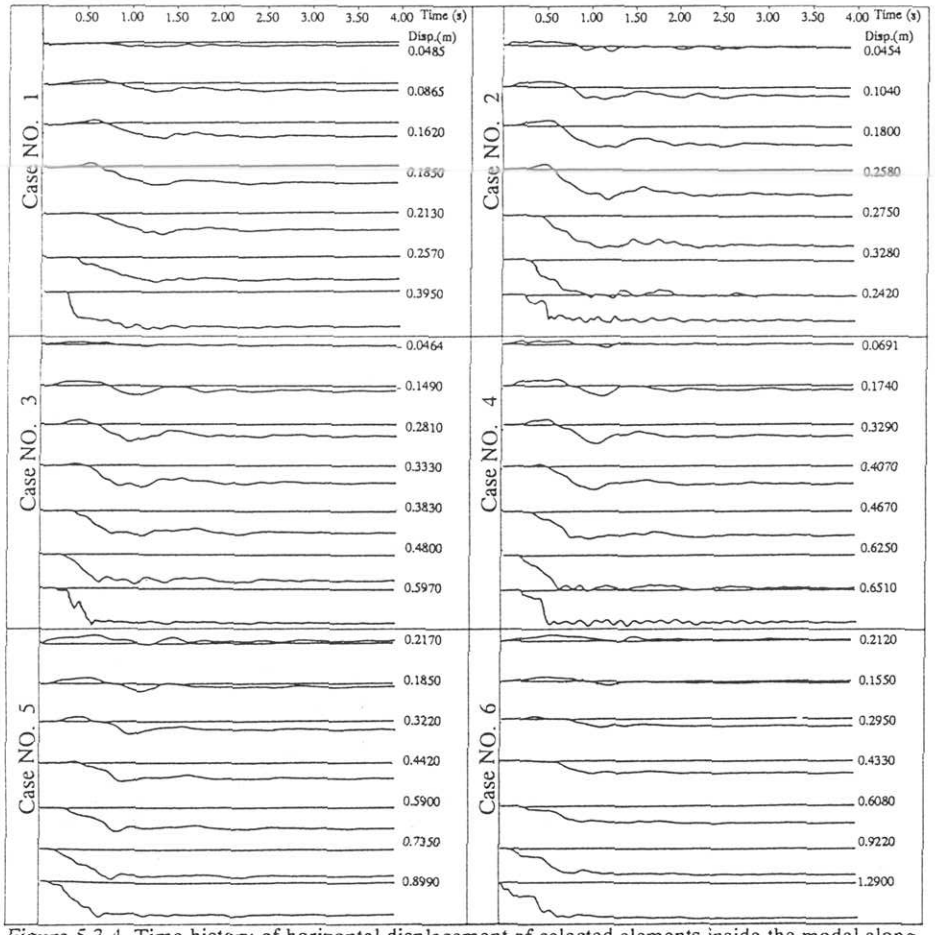

Figure 5.3.4 Time history of horizontal displacement of selected elements inside the model along different lines (see Figure 5.2.5)

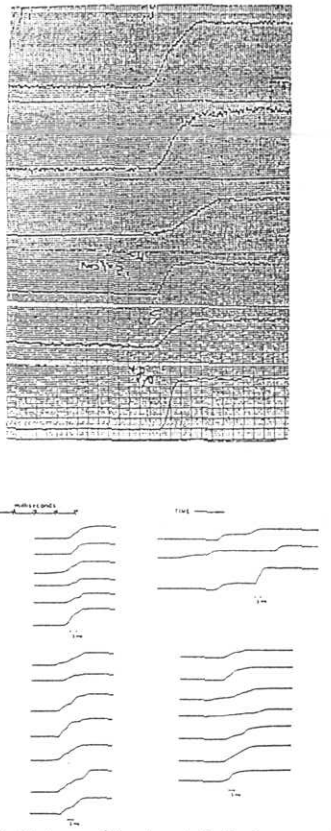

Figure 5.3.5 Nature of horizontal displacements near the fault of a foam rubber model for a qualitative comparison (after Brune, 1973)

approach, however, a linear function of time is generally used as the earthquake source-time function. The qualitative results obtained in this study also support other researchers' conclusions that, in reality, the source-time function has complicated shapes. The advantage of studies like this lies in the fact that we do not assume any shape of the displacement function at the outset, but obtain it as a natural consequence.

6. Studies of Rupture Propagation and Strength Barriers

6.1 General

As explained earlier, the physics of the collapsing rock masses in the environment of the Earth's interior are complicated so simplified assumptions are made and different phenomena are studied by many researchers using different approaches (see Das and Aki, 1977, for example). For example, the circumstances of rapid fracture spread, as well as the circumstances of fracture arrest are of interest to seismologists. As distinct from the engineering discipline, seismological studies demand a study of the growth of a large number of fractures in a heterogeneous medium. The strength heterogeneity of the medium is primarily responsible for the arrest of a fracture. The mechanism of the cessation of a fracture also constitutes an active area of research by itself. Arresting a rupture with a strength barrier, beyond which is an area under high stresses, causes the process to linger with strong aftershocks. Extending the fault to the area under low average stresses is responsible for fault cessation.

In this section, the Extended Distinct Element Method (EDEM) is used—for the first time—to study rupture propagation, its encounter with various types of strength barrier and the mechanism of cessation. The primary objective is to introduce the EDEM as a new tool to studying some of the complicated mechanisms of earthquake source process. This method, as has been described earlier, is capable of modeling the behavior of a medium from a continuous state to a discontinuous state following the total fracture process. Therefore, phenomena in which there are large displacements and appearance of cracks inside the medium can be very conveniently analyzed by this method.

The model used consists of circular elements—all having a radius of 2.5 meters (see Figure 6.1.1). This is therefore the case of a geometrically homogeneous model. Phenomena conforming more to those observed in nature can be analyzed by rejecting the homogeneity hypothesis. In one case in this study, therefore, the inherent heterogeneity of the region is modeled using random material properties to simulate random-strength barriers.

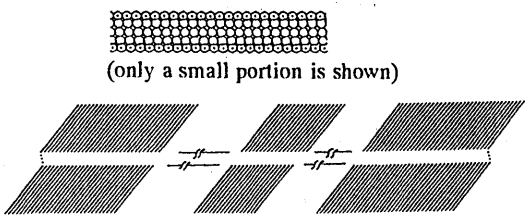

Figure 6.1.1 Model used to study rupture propagation and effects of strength barriers; the model consists of 1,500 circular elements—each having a radius of 2.5m—arranged in five rows. The length of the model is 1,500 m.

The critical parameters necessary for this study are obtained from trials after the model becomes ready for conducting the *numerical experiments*. The model is shown in Figure 6.1.1 with the associated dimensions.

6.2 Model Description and Preparation for Numerical Experiments

Model Description: To study rupture propagation, a model having a length of 1,500 meters and a width of 25 meters is prepared, and elements each having a radius of 2.5m are generated inside it. The total number of elements employed in this model is 1,500, with 894 inner elements and 606 support elements. The parameters for preparing the model are noted in Table 6.1.

Table 6.1 Parameters used for the rupture propagation studies by EDEM

Normal Direction			Shear Direction		
Element	Spring Constant ken (N/m)	9.0×10^{8}	Element	Spring Constant kes (N/m)	3.0×10^{8}
	Damping Constant cen (Ns/m)	2.0×10^{7}		Damping Constant ces (Ns/m)	1.2×10^{6}
Pore	Spring Constant kpn (N/m)	9.0×10^{8}	Pore	Spring Constant kps (N/m)	9.0×10^{8}
	Critical value α for setting pore spring	1.1		Critical value β for fracture of pore spring	1.10 (1.05)
				Cohesion	5.0×10^{12} (5.0×10^{9})
				Friction Coefficient	2.0 (2.0)

Preparation for Numerical Experiments: The bottom support (see Figure 6.1.1) is moved vertically with a constant rate displacement. The model is then brought practically to an *at -rest* condition by damping vibrations. Next, the bottom support is moved horizontally with a constant rate shear displacement and viscous damping is again used to bring the model practically to an *at rest* condition. The last two steps are performed to simulate the stressed stage of a crust just before a rupture occurs. These steps were outlined earlier in section five. After the model is ready for conducting numerical experiments, critical parameters are found at which cracks begin to appear inside the model. By parameterization, a rupture is incited at a critical location and the resulting rupture propagation is studied. For brevity, the critical parameters obtained after a few tests are noted inside brackets in the same table.

6.3 Study of Rupture Propagation

Progressive development of cracks from a region where rupture is incited by parameterization is studied in the following. The objective of this part is to study rupture propagation and effects of encountering the rupture with various types of strength barrier. Although such studies are performed by other numerical methods such as the finite element method (Toki et al., 1985) and the finite difference method (Miyatake et al. 1987), the EDEM has special merits over these numerical methods in that progressive

development of cracks inside a medium can be simulated automatically and as large displacements are possible during the analysis, new contact between the elements that were not previously in contact is naturally simulated.

Starting from the model in Figure 6.1.1, rupture propagation with and without the inclusion of a barrier region is presented in the following sections.

6.3.1 Case of Uniform Strength

As the first numerical experiment, a few cracks are created at the critical location, which is at extreme left of the model. The critical parameters are employed in the subsequent analysis. Figure 6.3.1 shows the occurrence of cracks in the model at several discrete time stations, with the bold lines denoting cracks whose cause is tension and the normal lines represent cracks due to the exceeding of shear strength.

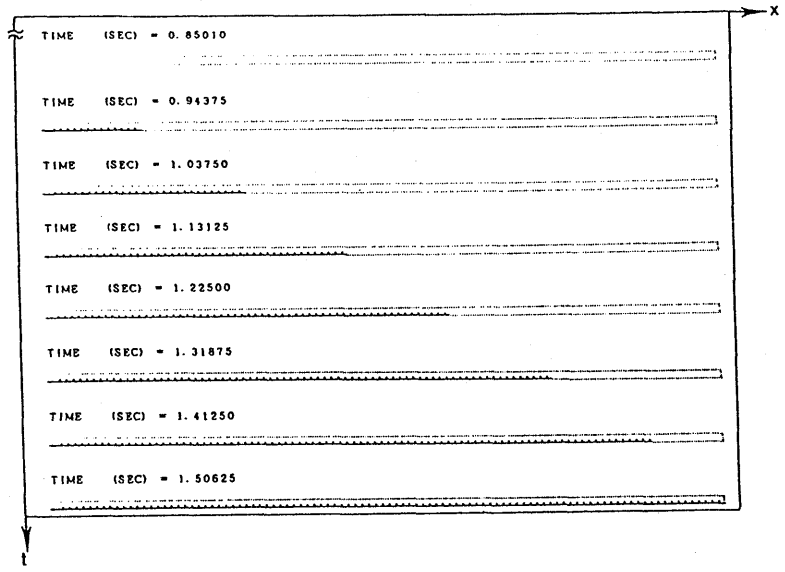

Figure 6.3.1 Progressive development of cracks (rupture propagation) in the standard case (no barrier is present). Rupture is incited at the bottom left corner of the model by instantaneously breaking a few pore-springs and utilizing critical parameters obtained from trials for the subsequent calculations.

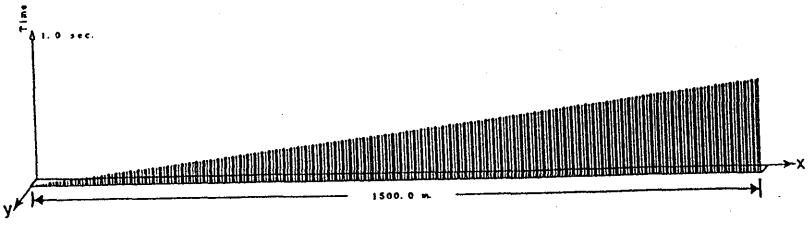

Figure 6.3.2 Crack location versus occurrence time (standard case, no barrier is present). The vertical ordinate represents time elapsed after the rupture is incited at the left bottom corner; the horizontal sides represent the model dimensions.

It can be clearly seen that the cracks are propagated with an almost constant rupture velocity, which can be readily computed from the slope of the line in Figure 6.3.2, of approximately 2.76 km/s. The compressional wave velocity assumed at the outset for determining the necessary parameters is 3.05 km/s. The rupture velocity is V_r = 2.76 km/s, which is almost 90 % of the compressional wave velocity in the present case. This apparently high value of rupture speed may be attributed to tensile strain in the elongated pore-springs and the use of the critical values of parameters. In a later part (see Section 7), the pore-springs are brought to have compressive forces by altering the model again and the rupture velocity without the occurrence of any tension cracks is found to be approximately equal to 2.2 km/s.

6.3.2 Experiments with Strength Barriers

Strength heterogeneity of the medium primarily responsible for arresting the fracture is studied in this section. Starting from nearl the middle of the model, the right-half of the model is taken as a barrier region. In the first case, the barrier region is made stronger than the left (uniform) part by increasing strength parameters, namely, the C_{EDEM} and β_{cr}, with a fixed percentage. In the second case, the same barrier region is treated as having random strength by distributing the strength parameters uniformly over some range.

6.3.2.1 Strength Barriers of Fixed Strength Ratios

After the cracks are allowed to propagate until a certain length in section 6.3.1, a

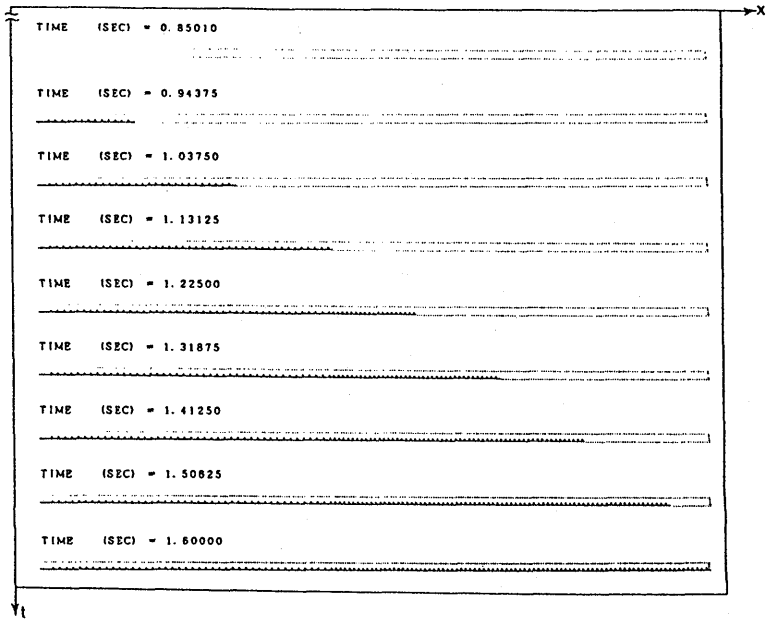

Figure 6.3.3 Progressive development of cracks (rupture propagation) in the 10% strong barrier case. Rupture is incited at the left bottom corner of the model by instantaneously breaking few pore-springs.

strength barrier is introduced by making the strength parameters, viz., cohesion and friction angle, of the remaining part of the model successively 110%, 120% and 130% in three different tests. Figure 6.3.3 shows the progressive development of cracks (rupture propagation) in the 10% strong barrier case. Rupture is incited at the bottom left corner of the model. When compared to the standard case of Figure 6.3.1, it can be noticed that the tip of the crack has advanced a smaller distance at the same time, for example, at time = 1.50625 sec. Therefore, the rupture speed, which is nearly 2.27 km/s, is seen to have reduced in this case due to inclusion of the strength barrier inside the model.

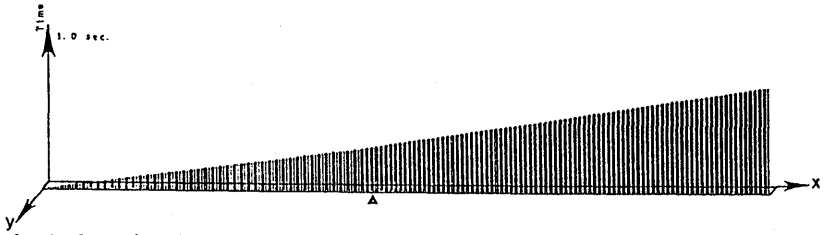

Figure 6.3.4 Crack location versus occurrence time (10% strong barrier is present starting nearly at the center of the model). The vertical ordinate represents time elapsed after the rupture is incited at the bottom left corner; the horizontal sides represent the model dimensions.

Figure 6.3.4 shows the crack location versus time of occurrence for this case. The position where barriers start is also noted in this figure. The vertical ordinate in this figure represents time elapsed after the rupture is incited at the bottom left corner of the model. Figure 6.3.5 shows the progressive development of cracks (rupture propagation) in the 20% strong barrier. Again, the rupture speed is seen to have further reduced to approximately 1.8 km/s because of the inclusion of a strength barrier of a higher strength. In figure 6.3.6 there are two plots for the cases of 20% and 30% strong barriers. In the latter case, however, few cracks occurred and the rupture ceased to propagate (see the lower figure).

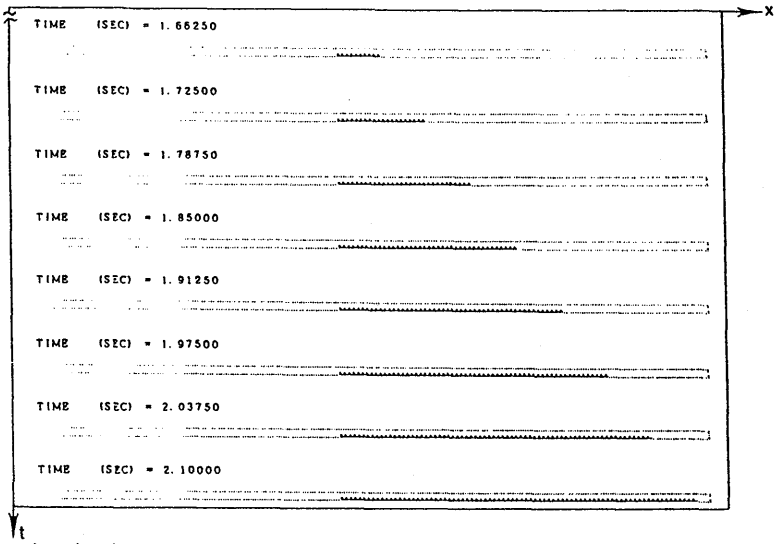

Figure 6.3.5 Progressive development of cracks (rupture propagation) in the 20% strong barrier case. Rupture is incited at the bottom left corner of the model by instantaneously breaking few pore-springs.

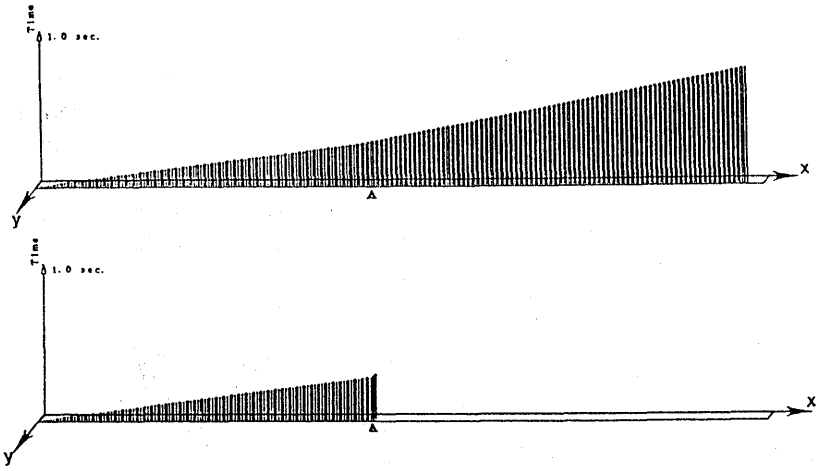

Figure 6.3.6 Crack location versus occurrence time (20% and 30% strong barriers start nearly at the center of the model). The vertical ordinate represents time elapsed after the rupture is incited at the bottom left corner; the horizontal sides represent model dimensions.

Combining all these results, Figure 6.3.7 shows the rupture velocities of all cases. It is clearly seen from this figure that rupturing is slowed as it encounters regions of higher and higher strengths.

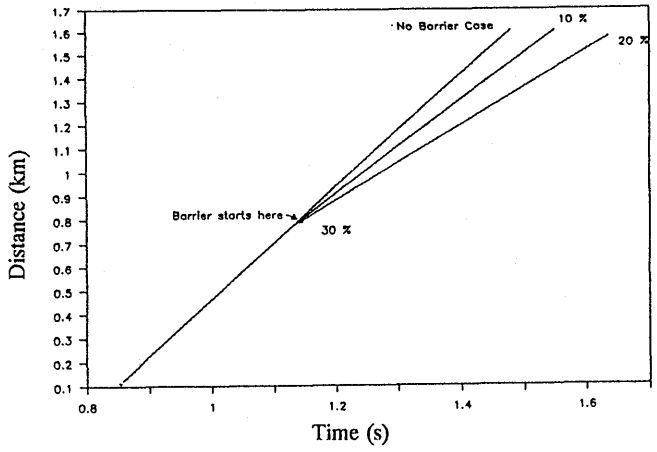

Figure 6.3.7 Crack location versus occurrence time (standard case as well as 10%, 20% and 30% strong barrier cases). The barriers start nearly at the center of the model. Slope of the line gives the rupture speed in each case.

Rupture velocity in each case is simply the slope of the corresponding line in the plot. When the strength of the barrier is 130%, the cracks could not penetrate, although very few cracks occurred at the beginning. Distribution of total force vectors in Figure 6.3.8 shows the propagation of total force taking place although no cracks could penetrate the region.

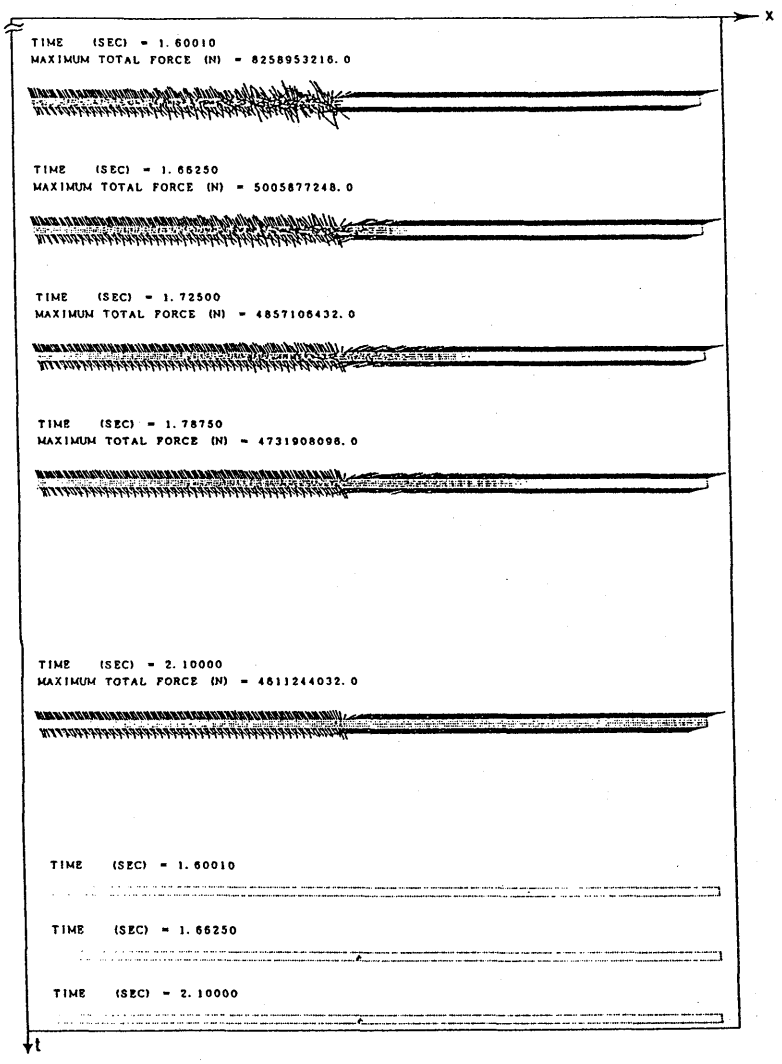

Figure 6.3.8 Total force vectors at selected time stations (30% strong barrier case). Because the barrier is too strong, rupture propagation could not occur; the total force, however, is seen to have transmitted from the figure (also see the lower figure for distribution of few cracks that occurred in this case).

6.3.2.2 Strength Barriers of Random Strength Ratios

Next, instead of making the remaining part of the model a region of uniform strength barrier as described earlier, random strength barriers are created over this non-ruptured part. The strength parameters, cohesion and friction angle, were allowed to vary randomly (uniform distribution) over the remaining non-ruptured region within the range 100-150%. This case resulted in few interesting results:

a) The rupture slowed at locations with higher strengths and accelerated at locations with lower strengths thus giving a zigzag pattern in the rupture time-location plot (see Figure 6.3.9 and top of Figure 6.3.11).

b) There were regions left intact at the beginning, but ruptured at later time stations. This may be attributed to higher stress concentration which exceeded the strength of the barrier (see Figure 6.3.10).

c) The rupture progressed for some time and finally stopped when it encountered a stronger barrier.

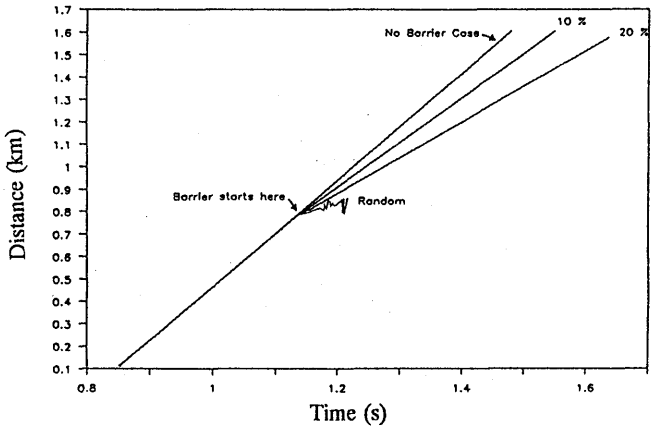

Figure 6.3.9 Crack location versus occurrence time (standard case as well as 10%, 20% and random (range 10-30%) strength barriers for comparison). The barriers start nearly at the center of the model. Slope of the line gives the rupture speed in each case. In case of the random barrier case, the cracks are seen to have propagated inside the region in a zigzag manner.

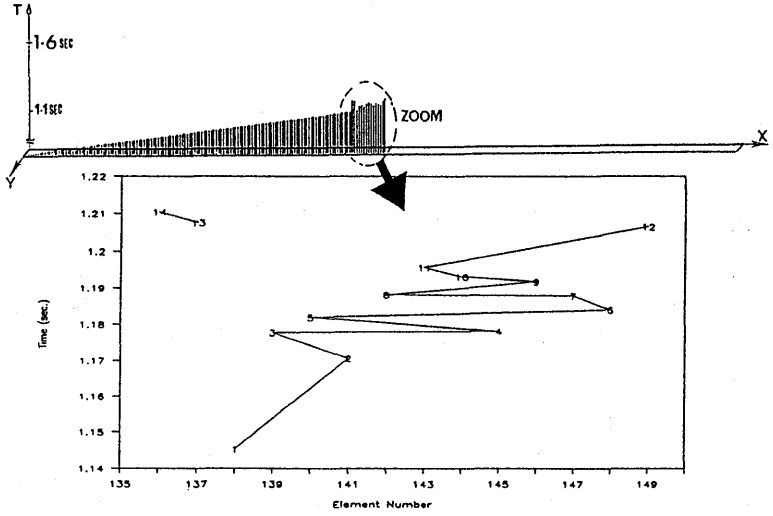

Figure 6.3.10 Crack location versus occurrence time (random strength barrier case). Also evident from these figures is that few initially unbroken regions are ruptured at a later time.

These observations are analogous to the real earthquakes in that the unbroken patches of the barriers correspond to the future locations of aftershocks.

7. Study of Mechanism Initiating Rupture

7.1 General

Earthquake rupture starts at a point inside the earth's crust where the stress becomes critical and exceeds the strength of the rock in its vicinity. A plausible assumption may be that the normal stress σ_{eff} in the equation $\tau = c + \mu \sigma_{eff}$ decreases due to an increase in the pore-water pressure resulting in a reduction of the shear strength. Based on such assumption, the Extended Distinct Element Method (EDEM) is used to study the rupture initiation mechanism using a model with the same geometry as that discussed in section 6.

7.2 Model Preparation and Numerical Experiments

In section 6, the model consisted of pore-springs that were under tension, which did not allow us to have independent control of friction. In the criterion of shear failure given by $\tau \leqq c + \mu \sigma_{eff}$, the second term at the right hand side of the inequality is not present when there is tension in the pore-spring. This modification led to success in studying the mechanism that starts a rupture which is explained in the following sections. The starting of the rupture can be attributed to exceeding of a critical shear strength S which takes into account friction μ and cohesion c.

7.3 Study on Mechanism Initiating Rupture

Two numerical experiments were carried out to study the mechanism that starts a rupture. The purposes and ways these experiments were carried out is described next.

7.3.1 Triggering by a Second Crack Gradually Approaching an Existing One

The purpose of this experiment was to see the stress concentration near an existing crack and the mechanism that starts a rupture. First, one crack is created at the bottom center location of the model. This is done by reducing the shear strength parameters μ and C_{EDEM}. Critical parameters are employed in the subsequent analysis (see Figure 7.3.1).

This does not lead to the propagation of a rupture and only one crack is seen in the model. In the second step, viscous damping is used inside the model to stop vibration caused by this disturbance before the second crack is created somewhere. Figure 7.3.2 depicts the total force of reaction, FX, of the element just below the crack. The reduction of this force is due to the reduction of friction, thus creating this crack. At the end of the time axis, the force has become constant, showing that the model has stopped vibrating. A second crack is then created—first at a distance and by successively coming closer to the crack, until rupture propagation occurs. Every time the second crack is created in a trial, the model employed is the same—that having one crack at the bottom center.

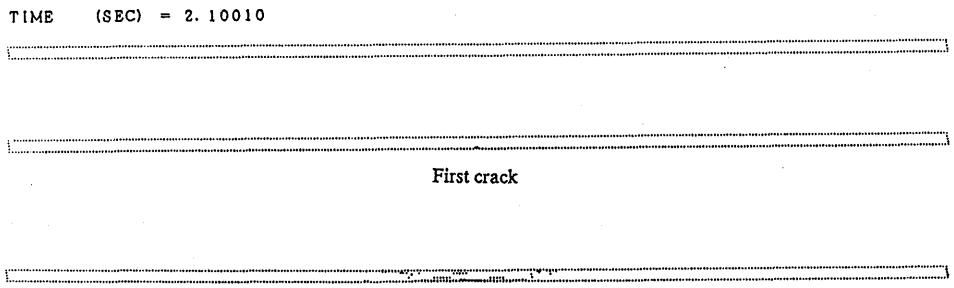

Figure 7.3.1 Simulation of start of rupture (Numerical Experiment case 1). One crack is created which alone does not incite rupture propagation. The bottom figure shows concentration of the shear force around this crack after the model comes practically to an *at-rest* condition.

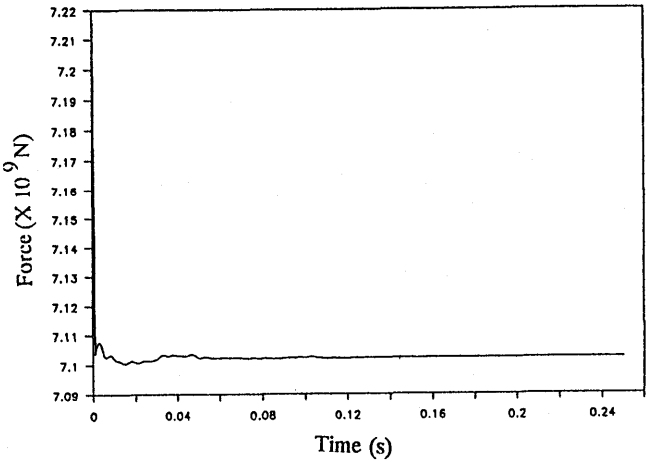

Figure 7.3.2 Drop of reaction force FX of the element due to rupture (Numerical Experiment case 1) seen after the model comes practically to an *at-rest* condition.

Observations and Discussions

Trial 1: The second crack was created at a location 100 elements farther to the left of the first crack as shown in Figure 7.3.3 (a). The concentration of shear force around the crack is seen in Figure 7.3.3 (b). No rupture propagation could be seen in this case, although there was an increase of shear force near the first crack due to the appearance of this second crack.

Trial 2: The second crack was created 10 elements farther to the left of the first crack. No rupture propagation could be seen in this case also, although there was an increase of shear force near the first crack due to the appearance of this second crack (see Figure 7.3.4, which shows that the forces are increased due to a second crack).

Trial 3: The second crack was created at a location which is 9 elements farther to the left of the first crack. From Figure 7.3.5, it can be seen that rupture propagates both

ways, taking a little longer time compared to other intervals between successive cracks.

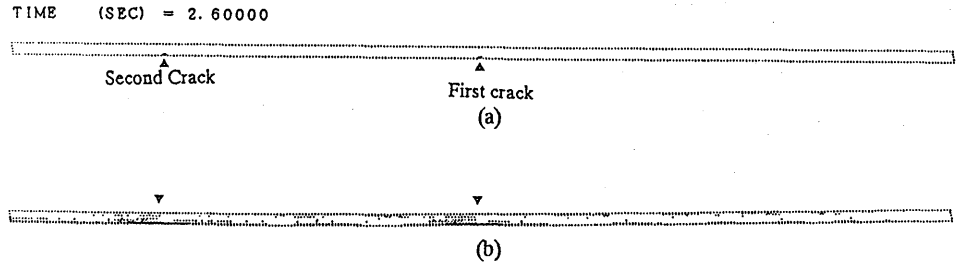

Figure 7.3.3 (a) A second crack created at a location 100 elements toward the left (above), and (b) shear force concentration near the cracks (below). The rupture did not propagate with this second crack as well (Numerical Experiment: case 1).

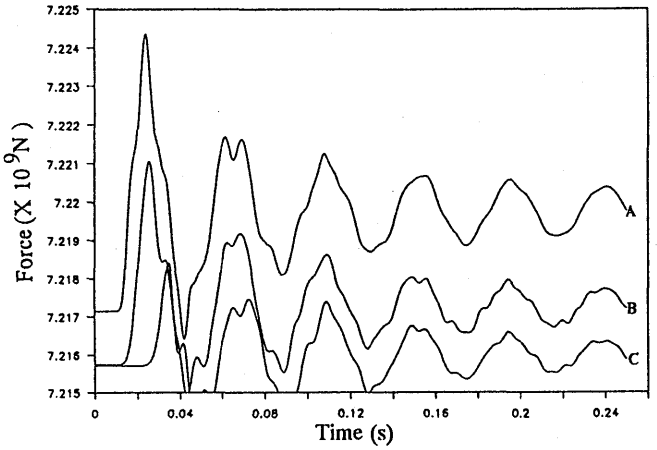

Figure 7.3.4 Distribution of total forces of reaction near the cracks (Numerical Experiment: case 1). A second crack created at a location 10 elements toward the left also could not start rupture propagation, but it can be seen that the force increases from the previous level in each of the three traces.

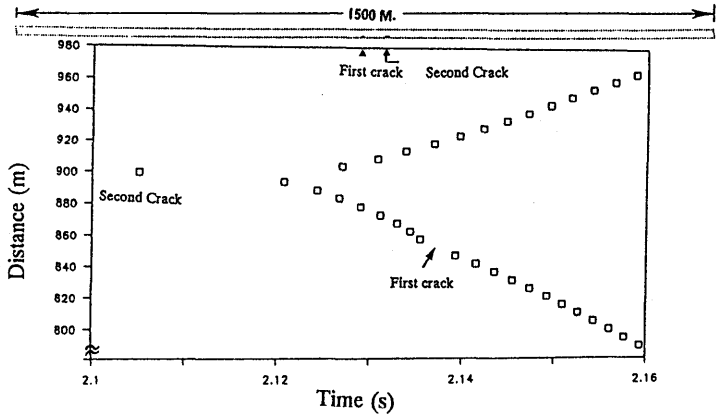

Figure 7.3.5 Rupture propagation occurred when the second crack was at nine elements farther from the first crack (Numerical Experiment: case 1). The rupture started after a small time has been elapsed and the nature of build-up of rupture speed is seen here to be nonlinear. Also, near the already existing crack, the speed gradually increases and then decreases. The upper figure shows crack locations inside the model.

Figures 7.3.6 show the total reaction force of selected elements at the base. It is seen that the forces increase before the rupture edge reaches the element and drop to a smaller value determined by friction. Figure 7.3.7 shows close-up views of the nature of increase of the forces before and after rupture.

Similar study has been done using the finite element method by Toki et al.(1985). Figure 7.3.8 qualitatively compares the nature of these forces with Toki's shear stress results.

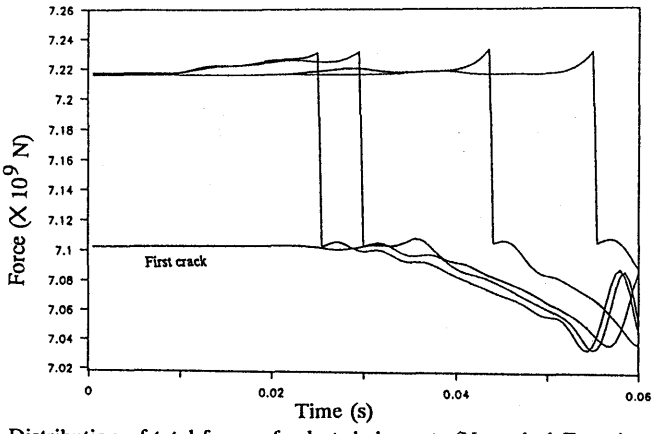

Figure 7.3.6 Distribution of total forces of selected elements (Numerical Experiment: case 1). The forces rise sharply just before the tip of the rupture reaches the corresponding region and drop to smaller values after being ruptured.

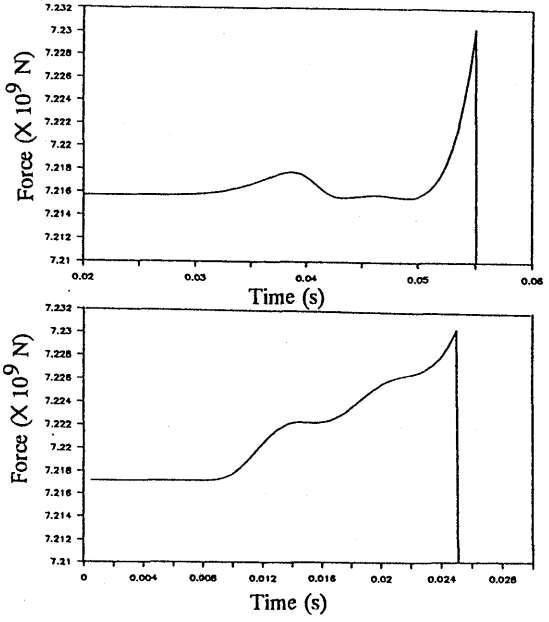

Figure 7.3.7 Close-up views of the nature of increase of the forces before and after rupture (Numerical Experiment: case1)

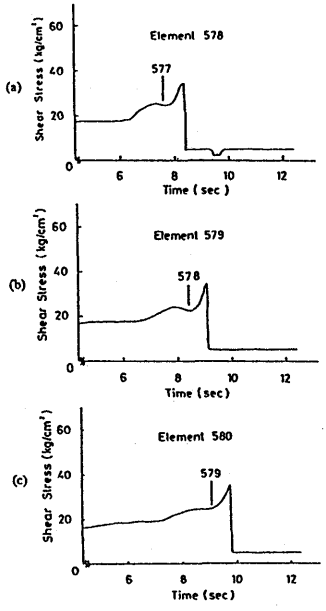

Figure 7.3.8 Nature of shear stress before and after rupture by finite element method (after Toki et al., 1985), for a qualitative comparison

7.3.2 Triggering Rupture by Creating Several Isolated Cracks

This experiment was carried out to study the mechanism that initiates an earthquake by following a series of steps which, in effect, simulate isolated events leading to a concentration of stresses near existing cracks before the actual earthquake. As shown in Figure 7.3.9, a pair of cracks was first created near both ends of model. This was found not to be sufficient to cause the rupture to propagate.

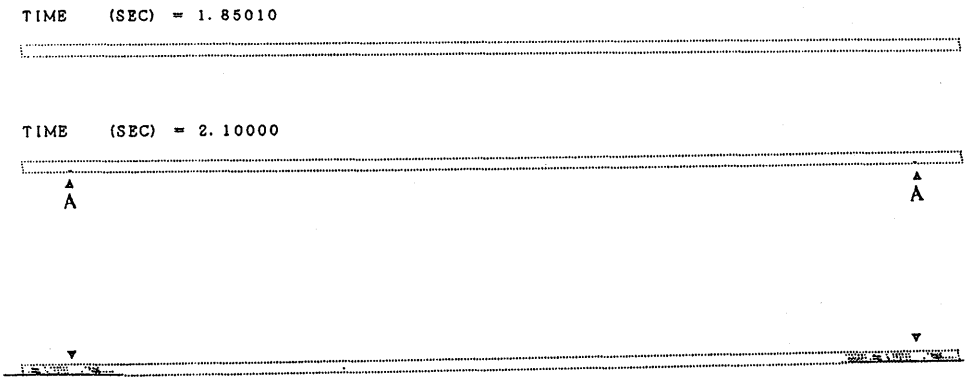

Figure 7.3.9 Pair of cracks created and shear force concentration near these cracks (Numerical Experiment: case 2). These cracks were not sufficient to cause rupture propagation.

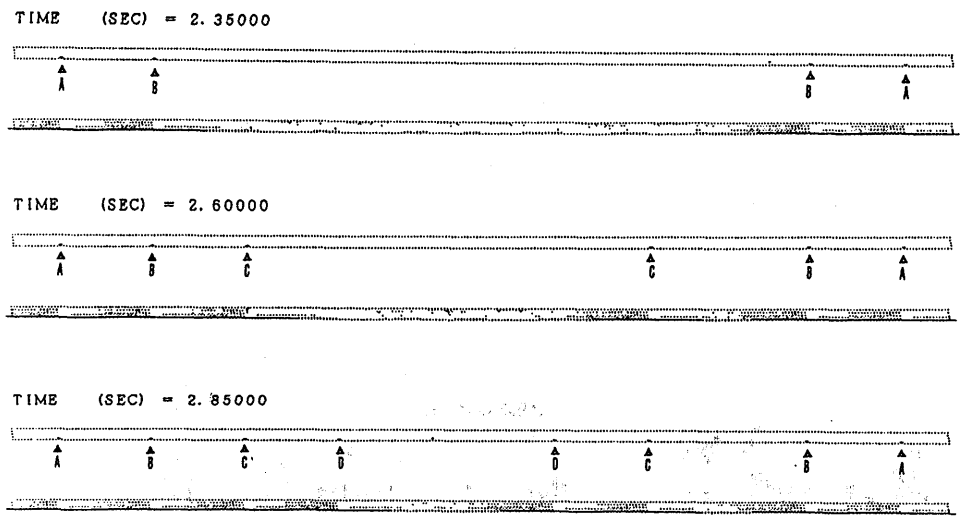

Figure 7.3.10 Cracks and shear stress concentration around them (Numerical Experiment: case 2). A total of eight cracks are present before the rupture started to propagate.

As the next step, the model was damped by making use of viscous dampers. The next figure shows the concentration of shear force in the region where this crack was

created. These steps were carried out until there were eight cracks, every time allowing the model to come practically to an *at-rest* condition by damping and Figure 7.3.10 shows the cracks and the shear force concentration around them after the model has been brought practically to an *at-rest* condition.

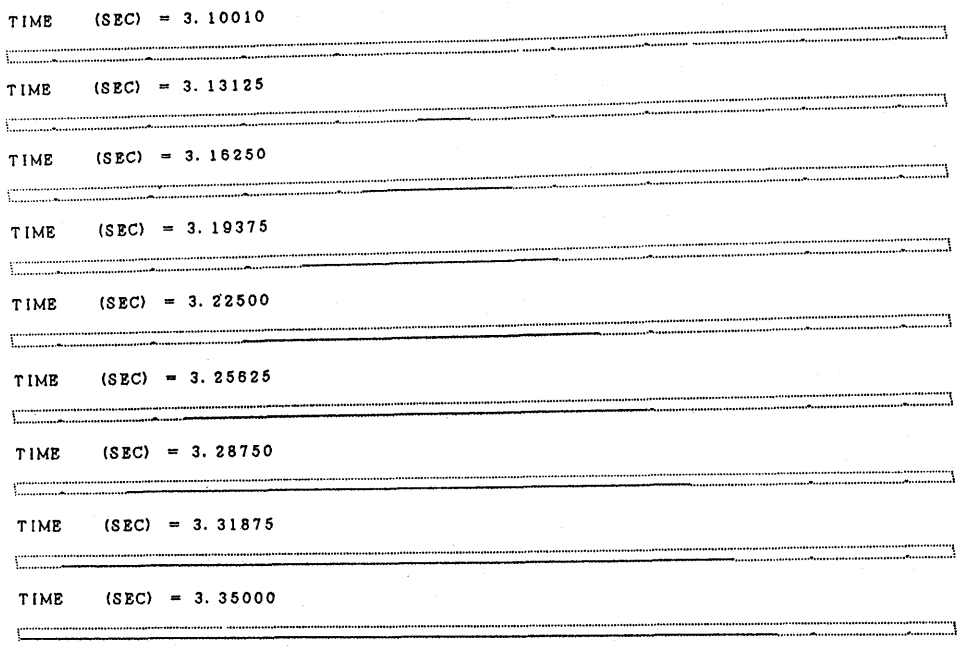

Figure 7.3.11 Progressive development of cracks after rupture starts by triggering (Numerical Experiment: case 2). A total of eight cracks are present before the rupture starts to propagate.

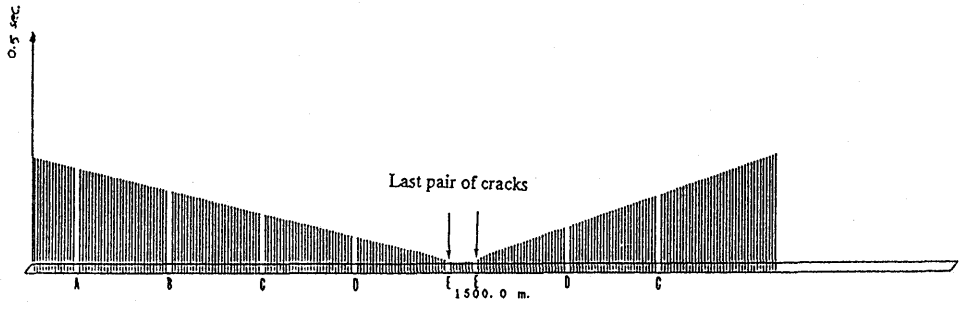

Figure 7.3.12 Location versus time of occurrence of cracks inside the model after rupture starts by triggering (Numerical; Experiment: case 2). A total of eight cracks are present before the rupture starts to propagate. It is seen that the start of rupture propagation takes longer time from the instant of triggering than the time elapsed between successive cracks after the rupture propagation has been started.

Rupture propagation was triggered by reducing cohesion – of two elements that are distant from each other and from the existing innermost cracks – to zero and keeping the same friction coefficient. Critical parameters were employed in the subsequent analysis. The rupture propagation started after a small time interval. Again, the rupture is seen to have propagated bilaterally in Figure 7.3.11 which shows the progressive development of cracks in the model at several discrete time stations.

Figure 7.3.12 shows a plot of location versus time crack occurred in this case. It is seen that the start of rupture propagation takes much longer from the instant of triggering than the time elapsed between successive cracks after the rupture propagation started.

Figure 7.3.13 shows close-up views of the nature of rupture propagation from which it can be observed that the nature of rupture speed build-up is nonlinear and that there is a change of slope (rupture velocity) near the existing crack.

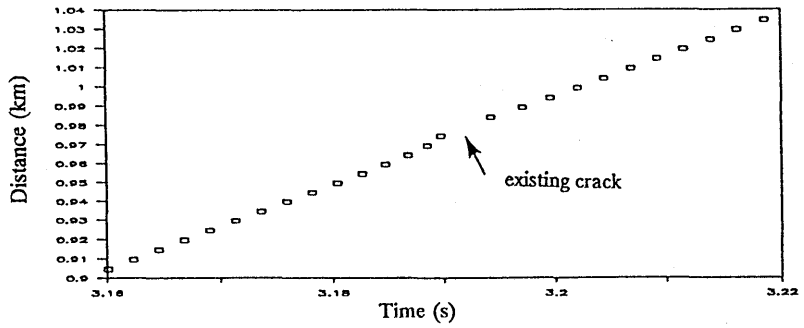

Figure 7.3.13 Close-up view of the nature of rupture propagation. In (a), the nature of the rupture speed building up is seen to be nonlinear; in (b) and (c), it can be seen that there is a change of rupture speed (slope of the curve) near the already existing crack.

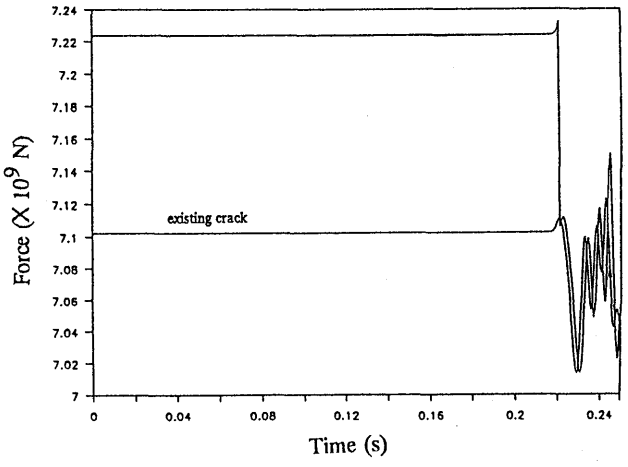

Figure 7.3.14 Force FX of selected support elements at the bottom row. These elements include both previously non-ruptured and previously ruptured regions (Numerical Experiment: case 2).

Figure 7.3.14 shows the reaction forces a few selected elements at the bottom of the model. These include elements which had already ruptured before triggering and for each of which there is already a drop of force. From this we see that the forces rise when the rupture edge nears the respective crack and drops to a lower level than the previous one. In this way, the simulation of stress drop due to rupture is simulated—for the first time—by the EDEM. Although the simulation results obtained are necessarily qualitative in nature, it has been shown that the EDEM shows great promise to help us understand some of the complicated mechanisms of the earthquake source process with the development of the method and computer systems.

8. Conclusions

The three approaches, namely, the theoretical, the experimental and the numerical approaches to studies of the earthquake source process, have been briefly discussed. In this study, the potential of the extended distinct element method (EDEM) as a suitable numerical tool to simulate a fracture of the Earth's crust has been demonstrated by applying this method to studying the earthquake source process-for the first time. Results such as progressive development of cracks inside a medium, dilatation and stick-slip type of forces have been obtained by applying displacement control on a few models. The frequencies of crack occurrences in a randomly heterogeneous model have been obtained for the first time by a numerical approach.

With the purpose of studying rupture propagation by the EDEM, the necessary steps to simulate critical conditions of the Earth's crust just prior to rupture have been developed. By parameterization, rupture has been incited at a location and the nature of displacements near the rupture and drop of shear force due to the occurrence of cracks have been closely observed. The total shear force is seen to have exhibited high frequency characteristics during the initial period of fracturing activity. Again, the EDEM has a strong advantage over other numerical methods in that progressive development of cracks inside the model and large displacements can be simulated in a very natural way. Consequently, new contact between elements that were not in contact before can take place, resulting in a new stress field inside the medium.

Next, by utilizing a long fault model and taking some measures, a critical condition simulating the Earth's crust just prior to the initiation of rupture has been realized. By inciting rupture at a critical location, the concentration of stress near existing cracks, the propagation of rupture from the disturbed region and its encounter with various strength barriers have been studied. It has been observed that the rupture speed slows when the barrier strength is increased and stops in the case of random strength barriers, leaving behind a few unbroken regions, which is analogous to the locations of future aftershocks in reality.

Finally, the mechanism starting a rupture has been studied by making two simulations. The nature of a rupture, its behavior near several existing cracks and drop of force due to rupture have been studied.

In spite of the qualitative nature of the results reported, it can nevertheless be concluded that with further development, the EDEM shows a great promise to help us understand some of the complicated mechanisms of the earthquake source process.

References

Aki K.: Seismic Displacements Near a Fault, *J. Geophys.Res.*,**73**, 5359-75, 1968

Andrews D.J.: Rupture Propagation with Finite Stress in Antiplane Strain, *J.Geophys.Res.*, **81**, 3575-82, 1976a

Andrews D.J.: Rupture Velocity of Plane Strain Shear Cracks, *J. Geophys.Res.*, **81**, 5679-87, 1976b

Brace W.F and Byerlee J.D.: Stick-Slip as a Possible Mechanism of Earthquakes, *Science*, **153**, 990-2, 1966

Brady B.T.: Theory of Earthquakes, 1. A Scale Independent Theory of Rock Failure, *Pure Appl. Geophysics*, **112**, 701-725, 1974

Brown S. R., Scholz C. H. And Rundle B. J. : A Simplified Spring-Block Model of Earthquakes, *Geophys. Res. Let.*, Vol. **18**, No.2, pp. 215-218, February 1991

Brune J. N. : Earthquake Modeling by Stick-Slip along Precut Surfaces in Stressed Foam Rubber, *Bull. Seismol. Soc.Am.*, Vol.**63**, No.6, pp.2105-2119, December 1973

Burridge R. and Knopoff L.: Model and Theoretical Seismicity, *Bull. Seismol. Soc.Am.*, Vol.**57**, 341-71, 1967

Cundall, P. A. : A Computer Model for Simulating Progressive Large Scale Movement in Blocky Rock System, *Symp. ISRM. Nancy, France, Proc.* Vol. **2**, pp 129-136, 1971

Das S. and Aki K. : Fault Plane with Barriers: A versatile Earthquake Model, *J. Geophys.Res.*, Vol.**82**, No.36, pp.5658-5670, December, 1977

Dieterich J. H. : Modeling of Rock Friction: Simulation of Preseismic Slip, *J. Geophys.Res.*, Vol.**84**, No. B5, May 1979

Hakuno M. and Hirao : A Trial related to Random Packing of Particle Assemblies, *Proc. of JSCE*, No.**219**, pp.55-63, 1973 (in Japanese)

Hakuno M. and Tarumi Y.: A Granular Assembly Simulation for the Seismic Liquefaction of Sand, *Structural Engineering/Earthquake Engineering*, Vol.**5**, No.2, 333s-342s, October 1988

Iida K. : Velocity of Elastic Waves in a Granular Substance, *Bull. Earthq. Res. Inst.*, Tokyo University, Vol. **XVII**, pp.783-807, 1939

Iwashita K. and Hakuno M.: Modified Distinct Element Method Simulation of Dynamic Cliff Collapse, *Structural Engineering/Earthquake Engineering*, JSCE, vol.**7**, No.1, 1990

Kasahara K. : The Nature of Seismic Origins as Inferred from Seismological and Geodetic Observations (1), *Bull. Earthq. Res. Inst.*, Tokyo University, Vol. **35**, pp.473-532, 1957

Kasahara K.: *Earthquake Mechanics*, Cambridge University Press, 1981

Kishinoue F.: Frequency-Distribution of the Ito Earthquake Swarm of 1930, *Bull. Earthq. Res. Inst.*, Vol. **15**, Part3, pp. 785-827, 1937

Knopoff L.: Energy Release in Earthquakes, *Geophys. J. MNRAS*, **1**, 44-52, 1958

Kostrov B.V.: Self-similar Problems Propagation of Shear Cracks, *J. Appl.Math.*, **28**, 1077-1087, 1964

Madariaga R.: Dynamics of an Expanding Circular Fault, *Bull. Seismol. Soc. Am.*, **66**, 639-666, 1976

Maruyama T.: Theoretical Model of Seismic Faults. *In Publications for the 50th Anniversary of the great Kanto Earthquake, 1923, Earthq. Res. Institute,* Tokyo University, 1 September 1973, pp.4147-65 (Japanese with English abstract)

Meguro K. And Hakuno M. : Fracture Analyses of Concrete Structures by Granular Assembly Simulation, *Bull. Earthq. Res. Inst.*, The University of Tokyo, vol. **63**, Part 4, pp 409-468, 1988 (Japanese with English abstract)

Meguro K. and Hakuno M. : Fracture Analysis of Seismic Fault by the Modified Distinct Element Method, *8th Japan Earthquake Engineering Symposium*, pp.145-150, 1990

Mikumo T. and Miyatake T.: Dynamic Rupture Process on a Three-Dimensional Fault with Non-Uniform Friction and Near-Field Seismic Waves, *Geophys.J.R.Soc.*, **54**, 417-438, 1978

Miyatake T.: Numerical Simulation of Earthquake Source Process by a Three Dimensional Crack Model, Part I, Rupture Process, *J. Phys. Earth*, **28**, 565-598, 1980a

Miyatake T.: Numerical Simulation of Earthquake Source Process by a Three Dimensional Crack Model, Part II, Seismic Waves and Spectrum, *J. Phys. Earth*, **28**, 599-616, 1980b

Mogi K. : Study of Elastic Shocks Caused by the Fracture of Heterogeneous Materials and its Relations to Earthquake Phenomena, *Bull. Earthq. Res. Inst.*, Vol.**40**, pp.125-173, 1962

Mogi K. : Magnitude-Frequency Relation for Elastic Shocks Accompanying Fractures of Various Materials and Some Related Problems in Earthquakes, *Bull. Earthq. Res. Inst.*, Vol.**40**, pp.831-853, 1962

Mogi K. : The Fracture of a Semi-Infinite Body Caused by an Inner Stress Origin and its Relation to the Earthquake Phenomena (Second Paper) - The Case of the Materials Having Some Heterogeneous Structures -, *Bull. Earthq. Res. Inst.*, Vol.**41**, pp.595-614, 1963

Mogi K.: Some Discussions on Aftershocks, Foreshocks and Earthquake Swarms- the Fracture of a Semi-Infinite Body Caused by an Inner Stress Origin and its Relation to the Earthquake Phenomena (Third Paper), *Bull. Earthq. Res. Inst.*, Vol.**41**, pp.615-658, 1963

Mogi K. : Earthquakes and Fractures, *Tectonophysics*, 5(1) (1967), pp.35-55

Mogi K. : Source Locations of Elastic Shocks in the Fracturing Process in Rocks(1), *Bull. Earthq. Res. Inst.*, Vol.**46**, pp.1103-1125, 1968

Mora P. and Donze F.: A lattice Solid Model for the Nonlinear Dynamics of Earthquakes, *Seismol. Res. Let.*, Volume **63**, No.1, January-March, 1992

Naiguang Geng, Jinsheng Hao, Jihan Li, Liu Xiaohong, Fang Yaru and Cai Daien : Stress Path and Frictional Sliding of Rocks, *Acta Seismologica Sinica*, Vol.**1**, No. 2, pp.93-100, March 1988

Ohnaka M. and Yamashita T.: A cohesive Zone Model for Dynamic Shear Faulting Based on Experimentally inferred Constitutive Relation and Strong Motion Source Parameters, *J. Geophys.Res.*, Vol.**94**, no. B4, pp.4089-4104, April, 1989

Propovics S. : Fracture Mechanism in Concrete: How Much Do We Know?, *J. Eng. Mech. Div.*, Proceedings of the ASCE, **EM3**, pp.531-544, June 1969

Rimal M. R., Meguro K., Hakuno M. and Higashihara H. : Study of Fracture of an Earthquake Fault Using the MDEM, *Proceedings of the JSCE Conference*, June 1991

Rimal M. R., Meguro K., Higashihara H. and Hakuno M.: Earthquake Rupture Simulation by Extended D.E.M., Proceedings of the 47th Annual Conference of the *JSCE* , vol.**1**, pp.1206, September, 1992

Rimal M. R., Meguro K. and Higashihara H. : Study of Fracture Process of an Earthquake Fault, *Proceedings of the 10th World Conference in Earthquake Engineering*, Madrid, July, 1992

Rimal M. R.: Dynamic Fracture Analyses by the Extended Distinct Element Method, A dissertation submitted in partial fulfillment of the requirements for the degree of Doctor of Engineering, Department of Civil Engineering, The University of Tokyo, September, 1992

Savage J.C. And Mansinha L. : Radiation from a Tensile Fracture, *J. Geophys.Res.*, Vol.**68**, No.23, pp.6345-6358, December, 1963

Scholtz, C. H. : The Mechanics of Earthquakes and Faulting, Cambridge University Press, 1990

Scholz C. H. : The Frequency-Magnitude Relation of Microfracturing in Rock and its Relation to Earthquakes, *Bull. Seismol. Soc.Am.*, Vol. **58**, No.1, pp.399-415, February 1968

Scholz C. H., Molnar P. and Johnson T. : Detailed Studies of Frictional Sliding of Granite and Implications for the Earthquake Mechanism, *J. Geophys.Res.*, Vol.**77**, no. 32, pp.6392-6406, November, 1972

Spetzer H., Sondergeld C., Sobolev G. And B. Salov : Seismic and Strain Studies on Large Laboratory Rock Samples Being Stressed to Failure, *Tectonophysics*, **144**, pp.55-68, 1987

Steketee J.A.: On Volterra's Dislocations in a Semi-Infinite Elastic Medium, *Can.J.Phys.*, **36**, 192-205, 1958a

Steketee J.A.: Some Geophysical Applications of the Elasticity Theory of Dislocations, *Can.J.Phys.*, **36**, 1168-1198, 1958b

Stuart W.S.: Diffusionless Dilatancy Model for Earthquake Precursors, *Geophys. Res. Let.*, **1**, 261, 1974

Takeuchi H. and Kikuchi M.: A Dynamical Model of Crack Propagation, *J. Phys.Earth*, **21**,27-37, 1973

Tarumi Y. and Hakuno M. : A granular Assembly Simulation for the Dynamic Liquefaction of Sand, *Natural Disaster Science*, Volume **10**, No.1, 1988, pp.45-59

Toki K. and Miura F.: Simulation of a Fault Rupture Mechanism by a Two-Dimensional Finite Element Method, *J.Phys.Earth*, **33**, 485-511, 1985

Wyllie L.: Performance of the Banco Central Buildings, *Proc., Conference on Managua , Nicaragua, Earthquake of December 23, 1972*, Earthquake Engineering Research Institute, Berkeley, California, 1975

Xiang chu Yin, Li Shiyu and Li Hong : On the Physical Essence of the b Value For AE of Rock Tests and Natural Earthquakes in Terms of Fracture Mechanics, *Acta Seismologica Sinica*, Vol.**1**, No. 4, pp.30-40, September 1988

Yamashita T.: On the Dynamical Process of Fault Motion in the Presence of Friction and Inhomogeneous Initial Stress, Part I, Rupture Propagation, *J. Phys. Earth*, **24**, 417-44, 1976

Zang Shaoxin and Jianli Fan : The Acoustic Emission and its Frequency Characteristics in Rocks under Different Types of Uniaxial Compression, *Acta Seismologica Sinica*, Vol.**1**, No.1, pp.86-101, December 1987

Zhiren Niu and Chen Dangmin : Slip-Weakening Instability on a Strike-Slip Fault with Asperity, *Acta Seismologica Sinica*, Vol.**1**, No. 3, pp.31-43, June 1988

Zhu C., Shukla A. and Sadd M.H.: Prediction of Dynamic Contact Loads in Granular Assemblies, *Journal of Applied Mechanics*, Vol.**58**, June, 1991, pp. 341-346